IEEE Access
Multidisciplinary ⋮ Rapid Review ⋮ Open Access Journal

Received 1 March 2023, accepted 16 March 2023, date of publication 22 March 2023, date of current version 28 March 2023.

Digital Object Identifier 10.1109/ACCESS.2023.3260213

TOPICAL REVIEW

Input Power and Effective Area in Terahertz Detector Measurement: A Review

ARIE PANGESTI AJI, CATUR APRIONO, (Member, IEEE), AND EKO TJIPTO RAHARDJO, (Member, IEEE)
Department of Electrical Engineering, Universitas Indonesia, Depok 16424, Indonesia
Corresponding author: Eko Tjipto Rahardjo (eko@eng.ui.ac.id)

This work was supported by the Seed Funding Professor Grant under Contract NKB-1938/UN2.F4.D/PPM.00.00/2022.

ABSTRACT The field of terahertz (THz) science and technology research area have been exponentially growing recently, motivated by the increasing demand for safer security imaging, better quality control within manufacturing industries, space and astronomical investigation, biomedical diagnostics, and larger communication bandwidth. The THz waves detection mechanism is one of the critical components in developing a high efficiency and high sensitivity THz communication system. This paper reviews the principle and instrumentation of THz optical metrology for the precise and accurate characterization of THz detectors in the range of 0.1 THz to several THz. In this context, we individually discuss the determination of radiation input power and effective area followed by a survey of THz optical measurement methodology used in the state-of-the-art THz detectors. In addition, challenging issues remaining in the THz detector measurements are provided. This paper sets out a guideline to address the main concept behind the THz detector measurement as well as their challenges and opportunities. Additionally, useful insight is given through a summary of available power meter instrumentation for THz input power calibration.

INDEX TERMS THz detectors, THz input power, effective area, THz metrology, antenna, THz measurements, THz instrumentation.

I. INTRODUCTION

Extensive studies by the global research community have been seeking for the prospective solutions to improve social life through the development of diverse and multiscale applications. A smart city concept to solve problems in the explosion of the urban population, a state-of-the-art automated non-destructive testing in the agricultural field, noninvasive imaging techniques in the biomedical field, and terabit per second data transfer for the next-generation communication system are among the recently reviewed technologies exploiting the benefit of the terahertz (THz) spectrum (0.1-10 THz) [1], [2], [3], [4].

THz radiation has gained enormous attention in the past couple of decades. It can interact with matters, penetrate materials like clothes, plastics, and wood, and reveal spectral information of abundant organic molecules. The millielectron volts (meV) photon energy of the THz waves is substantially lower than the energy of the chemical bonds, thus the ionization reaction is deficient. Therefore, it is safe for the application where human-body interaction is needed, such as security screening. The significant absorption by water in THz waves is also favorable as an excellent candidate to substitute X-ray imaging for detecting tumors and cancers. However, the aforementioned high-water attenuation makes the path loss severe in the THz range, where some frequency selectivity bands due to the molecular absorption can be confirmed and therefore limit the propagation distance [5].

Interest in THz radiation has been driven by the different physical phenomena revealed in this electromagnetic spectrum. Moreover, it also recalls multidisciplinary well-established knowledge in the electronics or photonics research area to develop components for THz wave generation. Thermal blackbody radiators, quantum cascade lasers (QCLs), photo mixers, and backward wave oscillators (BWOs) are some of THz sources developed based on photonic technology. As for purely electronic components is the microwave frequency multiplication based on Schottky

The associate editor coordinating the review of this manuscript and approving it for publication was Giorgio Montisci.

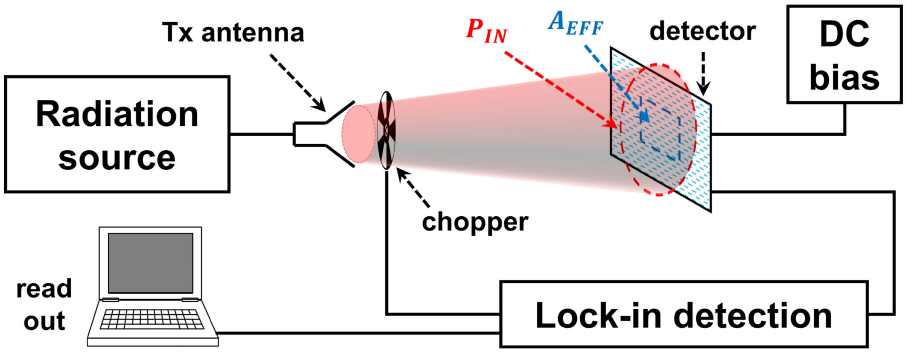

FIGURE 1. Block diagram of a THz detector optical measurement system. The THz signal can be modulated by either an external modulation connected to the source or a mechanical chopper in between transmitter and receiver, or internal modulator from the signal generator. The optical measurement involves the definition of radiation input power (P_{IN}) and normalization (effective) area (A_{EFF}) of the detector.

barrier diode [6]. The THz sources are able to radiate nano- to milli-watt power, where the higher frequency has the faster output power decay. The operational range can be chosen from a single frequency in the QCL-based source or narrow band frequency tunable-capable microwave generators and multipliers. A broad spectral range radiation up to the infrared region by the blackbody source is typically used to characterize the ultrawideband imaging system. On the other hand, THz detectors employ the detection mechanism based on different physical phenomena such as thermal, photon, or rectification by a nonlinear component. Relatively tiny size of detector components compared to the THz wavelength can be mitigated by integrating an antenna for a radiation absorber. Furthermore, THz detectors can be characterized either by mixing the terahertz signal with a different reference signal (heterodyne) or with the signal from the same source (direct detection).

The characterization of THz detectors requires careful attention for the precise measurement techniques. Unlike THz sources that can be characterized in a guided mode, THz detectors are measured in a free space propagation medium. The signal intensity at THz frequency is very low due to high propagation loss, intrinsic noise generated from detectors, and read-out circuits. Both electrical and optical approaches are necessary to define the measurement methodology. However, the electronic approach is limited by the high loss while larger wavelengths limit the optical one to some extent. Furthermore, significant molecular absorption and path losses in the atmosphere lead to only a maximum of a few meters of link distance between transmitter and receiver [7]. It is essential to get a high signal-to-noise ratio (SNR) output detector signal, which depends on the signal intensity, electronic and atmospheric noises, and detector sensitivity. Therefore, accurate THz detector measurement is a challenging task considering the typical detector output in the order of a few microvolts, and it is concealed in the intrinsic noise of the detector.

Fig. 1 shows a typical THz detector measurement block diagram which can be applied to any type of THz detector. The radiated signal can be modulated by internal or external modulation components as in the case of active imaging or radar, or unmodulated as in the case of a passive imaging system. The signal radiated from the source has the amount of power denoted by P_{IN} in which incident upon detector's effective area (A_{EFF}). The primary purpose of the detector's sensitivity measurement is to obtain the output signal as a ratio to the input power. The output signal can be detected by a lock-in mechanism to increase the SNR of the measurement. As for the input power, some techniques have been reported as part of a characterization process of THz detectors for both single- and arrayed-pixel configurations. Many THz detector measurements require an absolute measurement of radiant power in the THz region where the input power measurements are taken as synonymous with absolute commercial radiometers originally developed for THz wavelengths based on the principle of electrical substitution radiometry (ESR) [8]. For example, Ikamas et al. reported absolute responsivity measurement in the Si-CMOS FET detector by defining the input power from the all-electronic 0.6 THz source calibrated by a commercial Golay cell [9]. A similar method is reported by Bauer et al. using a large aperture area power meter [10]. However, some reports also require the sensitivity value based on the measurement of absorbed power in the detector in which the power is normalized according to the A_{EFF} of the detector calculated by measured antenna or detector physical parameters. For instance, a FET-based THz detector was reported by Zdanevičius et al. [11] with an effective area defined by simulated antenna directivity yielding 1.7 times larger area than its physical size. Another effective area definition based on its physical area is reported by Paulish et al. where the sensitive pyroelectric film area is used [12].

In this paper, we focus on the review of THz metrology in terms of THz detector measurement, emphasizing the input power parameter as the fundamental quantity in characterizing the THz detector. The input power on a THz detector characterization can be measured based on its radiated power and normalized area. Some THz detectors use different methods

TABLE 1. Comparison of THz detector review and survey papers.

Year	Detector Classification	Detector Type	Performance Metrics	THz Metrology	Ref
2011	×	HEB	✓	×	[13]
2011	✓	All	✓	✓	[14] ǂ
2015	✓	Plasmon-based	✓	×	[15]
2018	×	CMOS-based	×	×	[16]
2018	✓	All	✓	×	[17]
2018	×	All	×	×	[18]
2019	✓	All	✓	×	[19]
2020	✓	All	×	×	[6]
2020	×	All (commercial)	×	×	[20]
2021	✓	Si photonics	✓	×	[21]
2021	×	FET	✓	✓	[22] *
2021	✓	All	×	×	[23]
2022	✓	RTD	×	×	[24]
2023	✓	All	✓	✓	**This Work †**

ǂ Survey of THz input power measurement by commercial power meters
* Survey of different normalization area
† Survey of THz input power and normalization area

to measure the radiated power and effective area depending on the availability of the radiation source, optical components, or THz antenna measurement system. Here we report a guideline and survey on THz metrology, particularly radiation power measurement and effective detector area selections for THz detector characterization.

Previously, review papers on THz detectors have been reported in the THz research field area. Karasik et al. [13] reported the advance in fabrication techniques and required material synthesis for hot electron bolometers (HEBs), including the physics and technology used in the experiment. Additionally, the status of several other ultrasensitive detector concepts for the IR and far-IR wavelengths is outlined. Popović and Grossman [14] provided an overview of THz metrology used for the THz sources and detectors characterization. In particular, radiometry based on the free space and waveguide power meter is highlighted, and some available THz measurement instruments are provided.

Technological trends in modern THz detector research are reviewed by Otsuji [15]. The operation principles and characterization of several THz detector types are discussed with special attention given to the plasmon-type detectors. Marczewski et al. [16] presented an overview of the developments of CMOS-based THz detectors by some authors. The issues related to the influence of substrates, antenna, and transistor layout are discussed with examples of THz spectroscopy applications.

Sizov [17] gives a comprehensive survey on state-of-the-art THz detectors. The evolution of the basic classes of the THz detectors is highlighted in a wide range of detector types. Bogue [18] provides technical insight into the developments of THz sensing applications technology. The paper covers the discussion of the selection of THz sources and detectors. An overview of the recent commercial THz imaging applications is also provided. Lewis [19] proposes a taxonomy of THz detectors based on the underlying detection physical principles with a survey of the state-of-the-art detectors. A comparison of detector performances in terms of responsivity, noise, and response time performances is presented.

A review of applications, generation, and detection in the THz region is reported by Li et al. [6], where THz sources and detectors are classified based on the technology, providing an up-to-date reference for the researchers. Kasjoo et al. [20] presented an overview of THz imaging systems. Classification of imaging systems based on detection technologies is provided, including a survey on recently available applications in the market. Xie et al. [21] provided a review of THz technologies based on silicon photonics. The discussion includes the generation and detection scheme used in THz photonic-based components.

Javadi et al. [22] provided a review of FET-based THz detectors based on the effective area used for input power normalization. An experimental result based on the radiation power level measured by a commercial power meter is given. Lu et al. [23] conducted a study of integrated THz circuits and systems for different applications with emphasize on the review of integrated THz imaging systems in coherent, non-coherent, and near-field detection approaches. Wang et al. [24] presented an overview of room temperature THz transceiver technology for imaging applications. The authors emphasize the discussion on the non-linear characteristics of resonant tunneling diode (RTD)-based detectors and applications.

Of all the research work discussed above, only two discuss the perspective of THz detector measurements. However, in [14] radiation power measurement methodology is taken as absolute quantity based on a reference detector without further discussion related to the normalization area. As for the authors in [22] summarized the selection of effective area methodology specific for the FET-based THz detectors without discussing the input power calculation part. This paper provides the introductory guideline for THz metrology with an emphasis on THz radiation input power and effective area measurements. Numerous THz detectors are reviewed based on the input power and effective area calculation methodologies used in the measurements. Table 1 summarizes

the difference between this paper with other THz detector reviews.

The contribution of this work can be briefly outlined in the following items:

- Highlights the classification of the THz detector types
- Survey the input power and effective area methodology used in the THz detector measurement
- Provide open issues, challenges, and future research directions for the THz detector metrology.

The organization of this paper is as follow: Section II describes the classification of THz detectors according to different aspects, such as operation principles, detection mechanisms, and materials. The fundamental performance metrics, i.e., responsivity and noise equivalent power (NEP) are described in Section III. Section IV is the overview of THz detector measurement methodology, which consists of the definition of input power and effective area. Various implementations in the recent THz detectors are discussed. Section V points out several considerations in the THz detector measurement as well as open issues in the known methodologies. Finally, Section VI concludes the discussion.

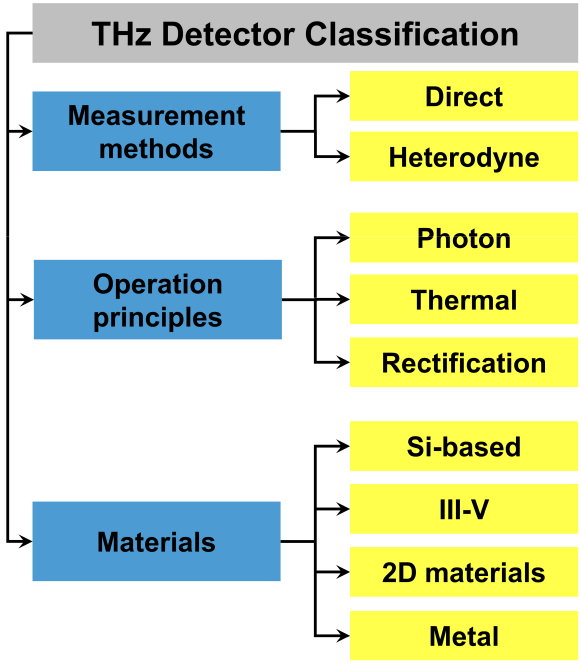

FIGURE 2. Classification of THz detectors.

II. TERAHERTZ DETECTOR CLASSIFICATION

In this section, the classification of THz detectors is discussed. To the best of the authors knowledge, there is no patented rule on how the THz detector can be classified, because different parameters have been used by researchers to categorize THz detectors. Here we summarize the classification of the THz detector based on three common parameters as shown in Fig. 2. The details of each detector class are discussed in the following subsections.

A. MEASUREMENT METHODS

THz detectors can be measured using two choices of measurement method, either direct or heterodyne circuits. The fundamental difference between the two is that direct detection measures only the signal output intensity, while heterodyne detection measures both the amplitude and phase of the field. Fig. 3 shows the comparison of measurement circuits for direct and heterodyne detection. In direct detection, the incident THz power is directly converted into a DC signal output without any conversion needed. The responsivity of direct detection can be improved with the use of an RF amplifier to boost the weak THz signal. In heterodyne detection, the incident high frequency (HF) signal in the THz range is downconverted into the lower intermediate frequency (IF) signal, usually in the microwave range [25]. This frequency conversion mainly relies on a nonlinear element device, such as a mixer and local oscillator (LO). The end product of the detector in the form of an IF signal can be further processed using backend electronic devices, i.e., a correlator, spectrometer, or total power detector.

For an imaging system, higher-quality images can be produced by a heterodyne imager. This advantage comes from the improvement of the received signal by the gain factor of the mixer and IF amplifier components, enabling the detection of weak signals. Moreover, the signal can also be boosted by a low noise amplifier before it is downconverted into an IF signal in the case of FET-based heterodyne imager at sub-THz applications [26]. However, additional noise contribution from the nonlinear components has a drawback in limited noise performance reduction compared with responsivity improvement capability. Moreover, a higher dissipated power is another issue in the heterodyne measurement system as a result of additional power-hungry nonlinear components. It is to be noted that the direct imager exhibits a broader bandwidth than the heterodyne imager. As long as the clarity of the image is the primary concern, a heterodyne imager outperforms the direct imager results. As an example, a heterodyne based on SiGe HBT THz detector is reported at 300 GHz, having a 50-fold responsivity improvement compared to the same device but with direct measurement. However, larger noise contribution in heterodyne detector impacts the NEP performance that can only be reduced by a factor of 5 [27].

The selection of circuit type between heterodyne or direct detection at THz spectral range depends on the application purposes, required detector sensitivity and speed, technological possibilities, spectral resolution needs, etc. An advantage of the direct detection systems is a simpler and compact measurement system with the possibility to design a large array format. Furthermore, it is suitable for detection in a shorter THz wavelength range. As for heterodyne detection offers a higher sensitivity in the lower THz frequency bands.

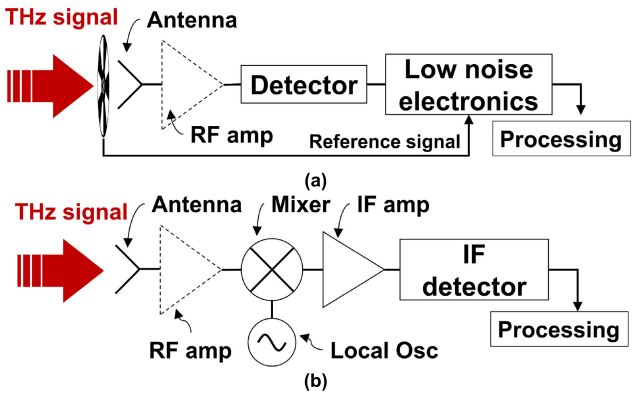

FIGURE 3. Measurement diagram of THz detector in (a) Direct detection and (b) Heterodyne detection.

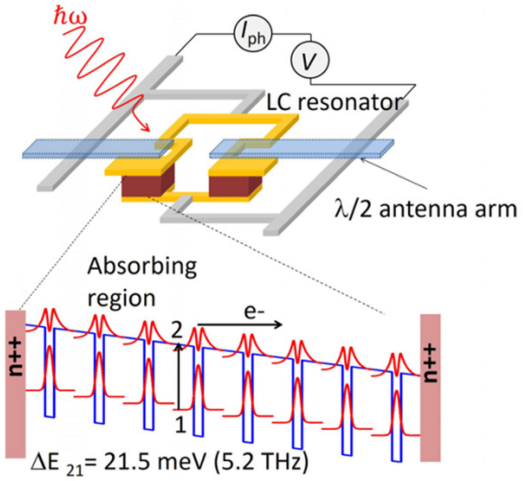

FIGURE 4. High temperature THz photon detector consist of quantum wells (QWs) and metamaterial based on LC resonator and patch antenna [35].

B. OPERATION PRINCIPLES

The second classification of THz detectors is based on the operation principle, including photon detectors, thermal detectors, and rectification detectors. The basic principle of photon detectors relies on the absorption of the incident radiation within the material by the interaction with electrons that are either bound to lattice atoms (intrinsic), impurity atoms (extrinsic) or free electrons. The electrical output signal results from the energy distribution change [28]. Typical photon detectors have the wavelength selectivity characteristics response per unit incident radiation power that favors photon detectors for shorter THz wavelength detection. As the energy per photon is inversely proportional to the wavelength, the spectral response of photon detectors increases linearly with increasing wavelength up to the cutoff wavelength point determined by the detector material. A common material used in an intrinsic photon detector is cadmium mercury telluride (HgCdTe) due to its bandgap tailoring characteristics. However, it requires a high cost for growth and processing. Moreover, the high rate of thermal carriers has made this material unsuitable for detection at f $\leq$ 10 THz [29]. Other material in photon detectors can be tailored based on the nature of the interaction, such as extrinsic detectors from the Ge semiconductor [30], [31], and quantum wells (QWs) detectors made of GaAs semiconductor [32], [33]. Photon detectors have a good signal−to−noise performance and a fast response in the IR and Far-IR regions. However, it is strongly limited by the thermal energy of the carrier, as the photon-generation rate should be larger than that of the thermo-generation rate to suppress the dark current noise. Therefore, the lower detection performance of the photon detector is expected at the THz region since the photon energy of 4 meV at 300 μm wavelength (1 THz) is very low compared to the thermal energy of 26 meV, assuming a room-temperature operation. An external cryogenic cooling mechanism can be used to prevent thermal generation in charged carriers, at the cost of a bulky and inefficient detection system [34]. A high-temperature THz photon detector is reported by Jeannin et al. [35] that combines eight QWs with the metamaterial architecture of the LC resonator and patch antenna, as shown in Fig. 4. The detector can be operated at 60K, which is higher than the typical QWs detector operation temperature.

A thermal detector absorbs the incident radiation, and a temperature rise in the material causes a change in some of its physical properties. Furthermore, the resultant change of physical properties is processed to generate an electrical output signal. In order to improve the rate of temperature rise (low thermal mass), thermal detectors are usually suspended on lags connected to the heat sink. In a thermal detector, the output signal does not have a dependency on the photonic nature of the incident radiation. Hence the performances are generally wavelength independent. Thermal conductance is an important parameter when developing a thermal detector, as the responsivity is inversely proportional to it. However, a slow heating process in thermal detectors resulted in a trade-off between responsivity and response time. Thermal detectors can be further subdivided into different approaches, namely pneumatic [36], bolometric [37], thermoelectric [38], and pyroelectric effects [39], with the independent material choices according to the selected approach. A pneumatic detector utilizes gas (e.g., xenon) in an enclosed chamber in which its volume is changing due to radiation heating that leads to displacement of the flexible membrane. As for bolometric, thermoelectric, and pyroelectric effects rely on the material with a high temperature coefficient of resistance (TCR), Seebeck coefficient, and pyroelectric coefficient, respectively. Recently, a combination of superconducting properties in niobium (Nb) and graphene has been shown as promising materials for bolometric-based THz detectors with an ultralow NEP performance as a result of the superconducting transition in the material junction, as shown in Fig. 6 [40]. Compared to photon-based detectors, thermal detectors have a moderate sensitivity due to the nature of the slow process in the thermal exchange. However, their

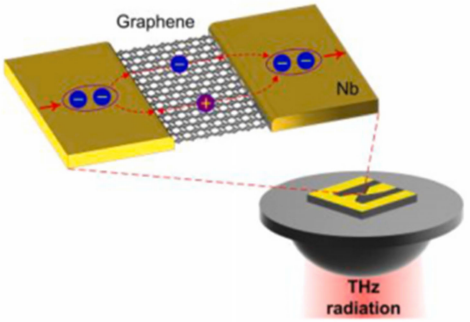

FIGURE 5. THz detector based on a Cooper pair transfers between superconducting Nb electrode via the graphene microbridge [40].

room-temperature operability is advantageous due to lower cost operation and compact size.

Rectification-based detectors process the incident electromagnetic signals in the elements of a nonlinear static current-voltage characteristic, leading to a rectification effect of the alternating current generated from the incident radiation. They can operate in a wide range of operating temperatures, broad spectral band, and can be characterized in both direct and heterodyne methods. Among some nonlinear rectifying devices, the most studied THz detectors are field effect transistors (FETs) and Schottky barrier diodes (SBDs). SBDs that have been used as a mixer for the heterodyne receivers in an astronomical application [41], [42], are now widely used as rectifying detectors, taking the advantage of nonlinearity in their current-voltage characteristic [43], [44], [45]. The initial study of the transistor as a nonlinear device for THz detection can be traced back to the research of plasma wave electronics by Dyakonov and Shur [46]. The photoresponse of FET-based detectors comes in the form of DC voltage between drain and source contact and is proportional to the radiation intensity. Another transistor type is high electron mobility transistors (HEMTs), consisting of a metal-semiconductor junction. Commonly used materials in a HEMT are aluminium gallium arsenide (AlGaAs) and gallium arsenide (GaAs), which provide a high level of basic electron mobility than Silicon FET. FETs and HEMTs are now favorable in the development of low noise and unbiased THz detectors. The fabrication technology readiness in Silicon and semiconductor foundry process have possessed a broad range of CMOS- and III-V material-based THz detectors [47], [48]. The fundamental limit in the rectifying detector is the parasitic effects generated from the electronic read-out components (resistors, capacitances, and inductances) that increase linearly with the frequency. The small sensitive area also another issue that makes the impedance matching to the radiation-receiving apparatus, such as the antenna, is challenging. Recently, a slot spiral type is reported as a good prospect to produce broadband characteristics at 0.15-0.45 THz. The antenna is coupled to a GaN/AlGaN HEMT detector (Fig. 5) and thus shows a sensitivity enhancement compared to a classic spiral antenna [49].

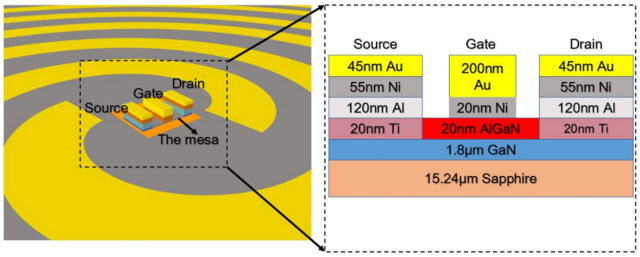

FIGURE 6. Slot spiral antenna coupled to a GaN/AlGaN HEMT detector with the source, drain and gate electrode are made of metals [49].

C. MATERIALS

The third THz detector classification is based on the detector material, including Si-CMOS-based detectors, III-V material-based detectors, two-dimensional materials, and metal detectors. In the last decade, complementary metal-oxide semiconductor (CMOS) foundry technology has been widely used for THz detector development. This technology allows easy integration of THz detectors with the readout circuitry. The fabrication can be either by using small Si foundry or extensive IC CMOS facilities, in which the former offers more degrees of freedom than the latter [16]. Standard submicron CMOS technology also provides the integration of several metallization levels, allowing the fabrication of a radiation absorber (i.e., antenna) a few micrometers above the substrate [50], [51]. Furthermore, a standard Si-CMOS THz detector is optimal for THz imaging [52]. Easy integration of Si-based FETs detectors with the readout circuitry is favorable for real-time mode cameras in the direct or heterodyne modes with a low production cost. Therefore, the CMOS fabrication technology is a productive and cost-effective solution related to sensors and compact imaging systems operating in the sub-THz region.

The research on III-V-based detectors started from the development of non-implanted GaAs, followed by the low temperature (LT) GaAs that allows the generation and detection of THz waves due to their picosecond's lifetime and high dark resistance [53]. Other III-V materials such as InGaAs compounds have the ability to operate efficiently with the telecom fiber lasers due to their narrow energy bandgap and cost-effective fabrication [54]. Furthermore, study of the compound materials based on InP- and GaN has been reported in which they have been integrated with HEMTs or Si-MOSFETs detectors in merged structures of gate electrodes and dipole antennas at 1 THz, resulting in enhanced responsivity beyond 1 kV/W [55], [56]. In addition, the adoption of multilayered structures of III-V materials revealed design flexibility, such as heat-spreading AlAs to improve the performance of conventional photoconductive layers [57]. After all, from the perspective of THz detectors, III-V materials are promising to increase device efficiency and sensitivity as a result of their high carrier mobility and absorption coefficient. The III–V detectors can also be monolithically integrated with silicon readout integrated circuits (ROICs) which offers significant opportunities for fully

functional CMOS-compatible photonic integrated circuit (PIC) technology.

The unique properties of 2D materials, such as graphene have incited the next-generation THz detectors. Since 2004, researchers have studied graphene material due to its unique property of linear dispersion relation between the energy and the wave vector [58], [59]. The use of graphene as THz detector material mainly includes the photovoltaic (PV) [60], bolometric [61], photoconductivity [62], and photo-thermoelectric (PTE) [63] effects. Other than graphene, 2D material photodetectors with similar detection mechanisms have been reported, such as MoSe2 photoconductor [64] which is based on transition metal dichalcogenides (TMDs) layered material, and black phosphorus (BP) [65] with ultrahigh responsivities. Those materials have exceptional physical and chemical properties, such as high light absorption due to quantum confinement towards vertical direction in 2D plane [66], broadband response due to their tunable bandgaps [67], and possibility of vertical heterostructure construction due to the absence of dangling bonds on its surface [68]. However, TMDs are limited for the detection in ultra violet (UV) to near Infrared (NIR) region due to their bandgaps, while BP can be tuned to THz region [69]. Furthermore, due to the long carrier lifetime in a two-dimensional layered material, there is a trade-off between sensitivity improvement and photo response speed. The selection of materials with high carrier mobility and low effective mass should be considered to mitigate the slow response time obstacle [69]. In addition to graphene, TMDs, and BPs, 2D material such as metal nitrides/carbides (MXenes) have grabbed much attention in the recent decade due to their intriguing properties of metallic conductivities, surface hydrophilicity, tunable bandgaps, and film thickness dependent characteristics in the range of UV, visible, and NIR spectra [70]. Moreoever, high absorption of Ti_3C_2 MXene ($\sim$160,000 cm^{-1}) has been investigated using density functional theory (DFT) calculation in THz region, indicating the potential of MXenes as THz detection materials [71]. Despite several years of widespread investigation of MXenes, research into MXenes material family is still in an early phase and report of THz detector based on this materials is yet to be found [70], [72].

The last THz detector classification is based on metallic materials, which are widely used as THz detectors aiming to their high temperature coefficient of resistance (TCR) characteristics. Hence it is susceptible against thermal radiation for room-temperature operation. Frequently used metal materials are a thin layer of Ni, Sb, Nb, Ti, Pt, or Pd. The metal materials are strong and have stable parameters which do not easily degrade over time. Furthermore, apart from the high value of TCR, the selection of metal should also consider the low noise and low thermal mass for high sensitivity thermal detector such as bolometer. Ti-based microbolometer arrays have been reported to have high sensitivity and are applicable for real-time operation at the THz region [73]. Even higher performance of metal detectors could be achieved by superconducting materials, where the metal has an infinite conductivity as a result of gradual resistance decrease below its critical temperature. Some metal superconductor-based bolometers have been reported such as YBCO [74], LSMO [75] and NbN [76] with ultralow sensitivity for Terahertz bolometric sensors. Metal materials also suitable for the THz detection employing thermoelectric effect. In this case, temperature difference is directly converted to a thermoelectric voltage output through the material property of Seebeck coefficient. Some metals with high Seebeck coefficient are Ti/Al (7.4 μV/K), Bi/Cr (70 μK/K) and Ti/doped Si (190 μV/K) [77]. In addition, pyroelectric materials such as lithium tantalite ($LiTaO_3$) ceramic materials and polyvinylidene fluoridehe (PVDF) are also exhibit temperature dependence characteristics that able to produce surface charges due to spontaneous electric polarization observed in the opposite polar axis of the material. Low emissivity and loss, high pyroelectric coefficient and low thermal capacitance, are among the important material properties for pyroelectric-based detector [78].

III. FIGURES OF MERIT

The working principle of a THz detector is to measure the change in the incident THz wave radiation into a measurable quantity such as current or voltage. During the measurement, various parameters must be considered and carefully controlled, including environmental, electrical, and radiometric conditions. Numerous textbooks and journals have discussed the figures of merit in an IR or THz detector [79], [80], [81]. Here we restrict our discussion to the responsivity and noise equivalent power (NEP) as the two main performance metrics that applied to any detector type. As for other figures of merit include spectral response, thermal response time, and the noise equivalent temperature difference (NETD) that commonly employed in thermal-based detectors, and detectivity in case of quantum well detectors [80].

A. RESPONSIVITY

Responsivity is a typical figure of merit for all THz detectors. It specifies the ratio of detector's output signal to the input signal radiated by the THz source. The input power of the terahertz radiation is expressed in the units of watts, and the detector output is an electrical potential difference between two terminals expressed in the units of volts. The root mean square (RMS) value is generally used as the fundamental component of input power and output signals. The responsivity ($\Re$) of a detector can be expressed by the following relation,

$$\mathcal{R}_v = \frac{V_{out}}{P_{in}} \tag{1}$$

where $\mathcal{R}_v$, V_{out}, and P_{in} are the voltage responsivity, voltage output signal, and radiation input power, respectively. As a matter of choice, if the detector's measurable quantity is the output current, the responsivity can be expressed as the current responsivity ($\mathcal{R}_i$). The radiation input power is

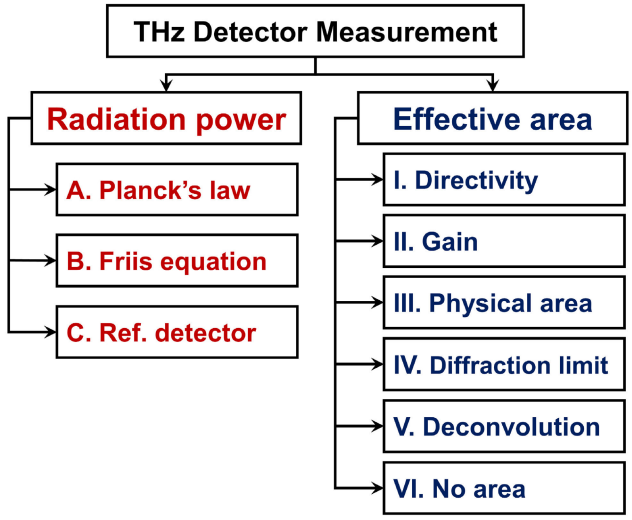

FIGURE 7. Classification of THz detector measurement methodology.

a general quantity applied similarly for any THz detector type. In contrast, the extraction of detector output signals is unique depending on the detection mechanism or measurement circuits. A spectral responsivity $\Re(\lambda, f)$ can be further defined by preference if the detector has a frequency (f) or wavelength (λ) dependence output signal. In this case, monochromatic radiation is used to illuminate the detector. However, one may also consider an absolute responsivity for a non-monochromatic source at one or a few frequencies utilizing a laser or calibrated source with the known power output. In general, a large value of responsivity is desirable.

B. NOISE EQUIVALENT POWER

The random fluctuation in the output signal caused by noise is unavoidable for any practical detector application. Even with the absence of radiation, the noise can still be present and contaminate the output signal. One may use the signal-to-noise ratio (SNR) to express the amount of noise in the output signal and set the limit of detection in a condition where the signal has the same size as the noise (SNR = 1). The noise equivalent power (NEP) defines the incident power on the detector that can generate a signal output equal to the RMS noise output. In another sentence, NEP is the signal level that produces a signal-to-noise ratio (SNR) of 1. The noise of a detector is measured at a specific frequency for a bandwidth of 1 Hz divided by the responsivity. The NEP can be expressed as

$$NEP = \frac{V_n}{R} \tag{2}$$

where V_n is voltage noise spectral density in the unit of V/Hz$^{1/2}$. The noise source can be varied depending on the operation principle, method of detection, and environmental condition during measurements. For example, a thermal-based detector is usually limited by the thermal fluctuation noise, while the shot noise limits a photon-based detector. A flicker noise dominates the detector response at low frequencies. Selection of the noise frequency is important to quantify the NEP. A frequency lower than the cutoff frequency is usually used to define the noise level where the detector response is independent of the low input modulation frequency range.

IV. TERAHERTZ DETECTORS MEASUREMENT

From the two main figures of merit discussed in the previous section, it is evident that accurate radiation input power measurement is fundamental in THz detector measurement. The optical input power is available at the interface between the detector and the free space medium. The measurement of actual power received by the detector is complex work since not all the radiated power is absorbed by the detector. It includes the losses caused by the reflection between the detector and the receiver antenna, polarization, and arrangement of the source and receiver antennas. This section discusses a comprehensive survey of THz detectors' optical input power measurement. The THz detector measurement methodologies are categorized based on their radiation power calculation and effective area. Fig 7 shows the classification diagram discussed in this section. The summary of reviewed reports on THz detector measurements will be given in the later section, which correlated to the classification shown in Fig. 7.

A. CALCULATION OF TERAHERTZ POWER

1) BY PLANCK'S RADIATION LAW

This method is primarily applied when a blackbody cavity is used as the radiation source in THz detector measurements [82], [83], [84], [85]. According to Planck's law, the temperature-dependent input power radiated from a blackbody source can be expressed as

$$P_{IN}(T) = \int_{\lambda_1}^{\lambda_2} \frac{2h^2}{\lambda^5} \frac{1}{\exp(hc/\lambda k_B T) - 1} d\lambda \tag{3}$$

where λ_1 and λ_2 denotes the lower and upper limit of spectral bandwidth of the detector, h is the Planck's constant, k_B is the Boltzmann constant, c is the speed of light, and T is the blackbody temperature in the unit of Kelvin. When the antenna is applied as the radiation absorber, the incident power can be calculated by integrating the blackbody power in the range of measured antenna bandwidth [84]. Alternatively, the transmittance spectra information of optical components such as mesh filters and a focusing lens located in front of the detector or spectral matching of receiver antenna can be applied to the calculation as the spectral bandwidth [83], [85]. Therefore, the radiation intensity can be reduced, aiming only at the power received at the center wavelength of the detector.

2) BY FRIIS TRANSMISSION EQUATION

In this method, the radiation input power is calculated based on the knowledge of transmitter antenna specification. The input power calculation by Friis transmission equation can

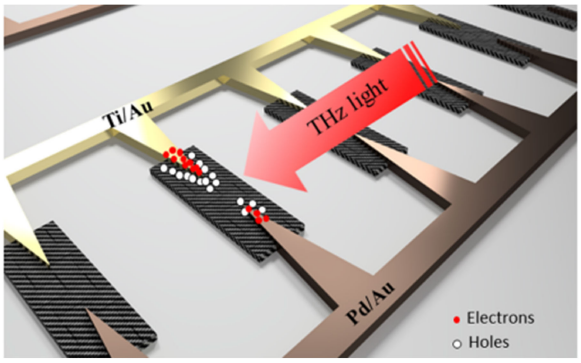

FIGURE 8. Physical graphene area at the center of bowtie antenna taken as the effective area where effective power is absorbed [123].

be expressed as

$$P_{IN} = \frac{G_T P_T}{4\pi r^2} \tag{4}$$

where G_T is the transmitter antenna gain, P_T is the amount of power radiated by the transmitter antenna, and r is free space distance between transmitter and detector plane. Most THz radiation sources employ a multiplier chain to generate THz power from the microwave range and a horn antenna with a typical gain ranging from 20 dB to 25 dB [86]. Additionally, losses from the optic components and antenna radiation efficiency can be accounted for more accurate estimation [87], [88]. Moreover, some reports also suggest the calibration of the power radiated from the horn antenna by a commercial reference detector in which the measured power includes the attenuation caused by path or optical losses [89], [90], [91], [92].

3) BY REFERENCE DETECTOR

In this method, a commercial reference detector is used to measure the radiated power at the same position as the detector under test, taken from the ratio of output voltage to the known voltage responsivity of the reference detector. The absorbed power by the detector can be estimated by multiplying the referenced power with the ratio of the effective area of the detector under test to the radiation beam spot from the source at the detector's plane [93], [94], [95], [96], [97]. Alternatively, suppose the opening aperture or area of the reference detector is much larger than the wavelength. In that case, the input power density can be extracted as a normalized value of the radiated power to the reference detector's area. In this case, the input power delivered to the detector can be taken as the multiplication of input power density with the effective area (A_{EFF}) of the detector under test [98], [99], [100], [101], [102]. Within this methodology, the precise specification of the radiation transmitter, as well as the distance between the source and detector can be neglected. As this approach measures the input power, which includes the path losses and optical attenuations, an accurate estimation of the impinging power can be given. Furthermore, the calibration of the reference detector is an important task prior to the measurement to get a precise estimation [103], [104].

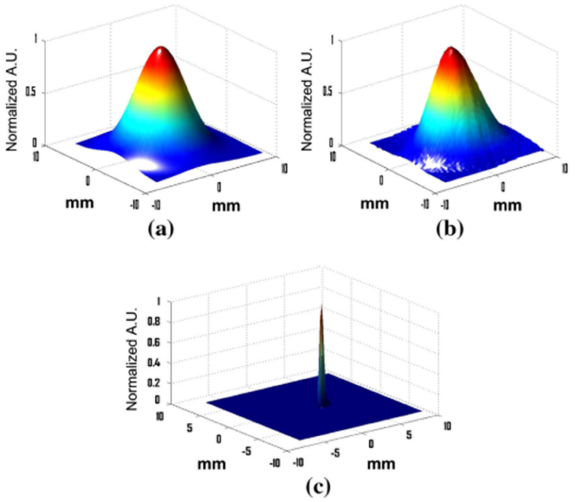

FIGURE 9. (a) Field distribution of incident Gaussian beam measured by knife-edge method, (b) Scan result THz radiation beam measured by antenna-coupled microbolometer under test, (c) detector's spatial response after the deconvolution using Richardson-Lucy algorithm [136].

B. DETECTOR NORMALIZATION AREA

1) ANTENNA DIRECTIVITY

This method defines the normalization area by the maximum effective aperture of the receiving antenna coupled to the detector. However, this method is valid under the assumption of a lossless antenna, and the impedance and polarization factors are matched in the wavelength region where the antenna operates. Thus, it is suitable for determining the responsivity based on the estimated power impinged to the detector area. If the maximum detector's antenna directivity (D) is known, the effective area can be expressed as

$$A_{EFF} = \frac{D\lambda^2}{4\pi} \tag{5}$$

with λ is the resonant wavelength of the antenna. The directivity value can be experimentally verified by plotting the antenna's radiation pattern in two projections of E- and H-plane and calculated based on the extracted full-width at half-maximum (FWHM) angles [22], [88], [105]. Moreover, some reports suggest the estimation of antenna directivity by electromagnetic simulation as a traceable methodology to calculate the effective area [106], [107], [108].

2) ANTENNA GAIN

This method is similar to the directivity-based effective area but contains information on the power losses due to antenna radiation and reflection efficiencies. Within this method, the power absorbed by the detector could be estimated. Knowing the gain (G) value of the receiving antenna, the effective area

TABLE 2. Silicon-based THz detectors measurements comparison.

Detector type	Frequency (THz)	Antenna	Responsivity (V/W)	NEP (pW/$\sqrt{Hz}$)	THz Optical Measurements		Pixel	Ref
					P_{IN} calculation	A_{EFF} method		
SiGe HBT 180 nm BiCMOS	0.32	Elliptical slot-ring	18k	34	C	III	Array	[113]
SiGe HBT 250 nm BiCMOS	0.7	Differential ring + lens	1 (A/W)	50	B	I	Array	[88]
SBD 130-nm CMOS	0.86	Rectangular patch	273	42	B & C	III	Array	[89]
MOSFET 90-nm CMOS	0.365	H-shaped dipole	185k	40	C	I	Single	[108]
Si MOSFET	0.2	Bowtie	222	-	C	III	Single	[93]
SiGe BJT 130 nm BiCMOS	0.26	Differential ring	2.7 (V/μW)	7.9	B & C	III	Array	[90]
Si MOSFET	0.2	Monolithic patch	842	18	n/a	III	Single	[116]
MOSFET 130 nm CMOS	0.82	Rectangular patch	3.46k	12.6	B & C	III	Array	[91]
MOSFET 65-nm CMOS	0.2	Rectangular patch	1.5k	15	n/a	III	Array	[117]
P-N Diode 45 nm CMOS	0.781	Rectangular patch	558	56	B & C	I	Single	[106]
MOSFET 130 nm CMOS	0.27	Bowtie	380	18.7	C	I	Array	[166]
MOSFET 130 nm CMOS	0.3	Bowtie	600	-	C	III	Single	[115]
HBT 130 nm SiGe	0.3	Dipole	322k (heterodyne) 6.1k (direct)	3.9 (heterodyne) 21.2 (direct)	C	VI	Single	[27]
MOSFET 65-nm CMOS	0.5	Differential patch	570	29	B	I	Single	[87]
MOSFET 150-nm CMOS	0.885	Bowtie	235	187	C	I	Array	[107]
Polysilicon MOSFET	0.65	Bowtie	600	200	C	III	Single	[127]
Si EIW	0.167	Dipole	3.3k	5.7	C	III	Single	[98]
MOSFET 90-nm CMOS	0 - 1.5	Log-spiral + lens	-	42	C	VI	Single	[161]
MOSFET 90-nm CMOS	0.609	Bowtie + lens	193	47	C	VI	Single	[144]
MOSFET 65-nm CMOS	0.62	Rectangular patch	1.4k	19.2	C	I	Array	[22]
MOSFET 65-nm CMOS	1	Double-quad + lens	765	25	C	VI	Single	[147]

can be calculated as,

$$A_{EFF} = \frac{G\lambda^2}{4\pi} \tag{6}$$

where the antenna gain and directivity are correlated with the efficiency factors [109]. Gain measurement has been widely used for the microwave band antenna, usually in a non-reflecting environment, using a known gain from a reference antenna (typically a horn antenna). However, gain measurement for the THz band antenna is quite challenging since one can hardly detach the individual contributions of the receiving antenna and the load components connected to it (e.g., detector). An estimation to justify the antenna gain improvement was proposed by Li et al., by using effective voltage responsivity based on two different detectors where the impedances are matched to the transmission lines connected to the antennas [110]. However, this method is difficult to be realized when the detector is directly connected to the antenna without a matching circuit. Alternatively, simulation-based antenna gain is generally used to calculate the effective area [111], [112].

3) PHYSICAL AREA

In the case of an imaging array with a multi-pixel imager, apertures of nearby pixels are overlapping each other. Hence the pixel aperture size can be reasonably taken from its physical or pitch size [113], [114], [115]. Some other works specify physical area from the actual detector area [116], [117], or active area [118], [119], [120], [121]. Note that the active area could also correspond to the thermal sensitive area where the change in the material physical parameter occurs that is caused by the absorbed radiation [122], [123], [124], [125]. A near-field probe was proposed by [126] in the form of a sub-wavelength aperture where the incident light can be focused on the detector and improve the spatial resolution.

TABLE 3. III-V-based THz detectors measurements comparison.

Detector type	Frequency (THz)	Antenna	Responsivity (V/W)	NEP (pW/$\sqrt{Hz}$)	THz Optical Measurements		Pixel	Ref
					P_{IN} calculation	A_{EFF} method		
InGaAs SBD	0.25	Square spiral	98.5	106	C	VI	Array	[139]
InAlAs HEMT	0.2 0.292	Dual-grating-gate	22.7k 21.5k	0.48	C	III	Single	[94]
GaAs QW	5	Patch	3.67 (A/W)	0.18	A	VI	Array	[82]
InP SBD	0.3	Bowtie + lens	3.2M	3	C	VI	Single	[160]
GaAs SBD	0.216	Log-periodic	563	1.2	B & C	VI	Single	[92]
AlGaN FET	0.59	Bowtie + lens	8	-	C	VI	Single	[153]
GaN Diode	0.29 0.66	Bowtie	2 0.2	-	C	VI	Array	[155]
InAs FET	3.4	-	2.5	4800	C	III	Single	[126]
AlGaN HEMT	0.14	Nanoantenna	15k	0.58	C	III	Single	[118]
InAs HBD	0.17	Folded dipole + lens	3.5k	1.48	C	VI	Single	[140]
AlGaN HEMT	0.9	Dipole + lens	-	1	C	VI	Single	[141]
InGaAs EIW	0.173	Dipole	515	20	C	III	Single	[97]
GaAs SBD	0.223	Bowtie + lens	2.19k	2.6	B	I	Single	[86]
GaAs Bolometer	0.25	MEMS resonator	-	500	C	VI	Single	[142]
InGaAs Photodetector	0.166	Log periodic	25	20	C	II	Single	[99]
AlAs RTD	0.78	Slot + lens	0.12 (A/W)	7.7	C	VI	Single	[148]
AlGaN HEMT	0.85	Dipole + lens	4 (A/W)	0.3	C	VI	Single	[143]
InSb Photodetector	0.171	Spiral	266k	0.022	C	II	Single	[111]

An example of an effective area definition by the detector (graphene) area is shown in Fig. 8, where the responsivity is based on effective power absorbed within the area [123]. In another report, a heavily doped resonant polysilicon antenna was proposed as a THz detector. Thus, the antenna cross-sectional area is chosen as the effective detection area where a strongly confined field is transferred to a FET detector [127]. It should be noted that the normalization of the incident THz radiation based on the physical sub-wavelength detector area would yield a higher responsivity value, due to the assumption that the THz power is focused into a such small area. However, this argument can be reasonably taken as long as the radiation beam spot size information is known, which usually has a much larger area. Thus, the impinged power can be taken as the power in the fraction of the physical area from the beam spot size.

4) DIFFRACTION-LIMITED AREA

This method has been reported for a more conservative estimation of detector performance. In the THz regime, the wavelength is larger than the detector size. Hence, it is also relevant for some research to use diffraction-limited area achievable by the relation of

$$A_{EFF} = \frac{\lambda^2}{4} \tag{7}$$

Some reports have used this method for the case of detectors without a dedicated antenna [128]. However, some other detectors coupled to the antenna also reported using this assumption, where there is no available measured or simulated information on antenna parameters such as directivity or gain [129], [130], [131], [132], [133]. This method is valid if the actual physical size of the detector is smaller than the diffraction-limited area in the wavelength operation. Thus, the responsivity is taken as the lower limit and can be actually larger if the traceable antenna measurement parameter is available.

5) DECONVOLUTION

With the physical size of a detector's pixel is generally much smaller than the incident beam spot in the THz range, it is fair to assume that the detector cannot absorb the total power radiated from the source. If the antenna is applied, the detector's physical dimension would also be smaller than the effective aperture of the antenna calculated by either directivity or gain. The deconvolution method involves numerical analysis of the THz radiation beam area in the focal plane of the detector ($S(x, y)$) measured by 2-D mechanical scanning. The measured beam contains the convolution of the detector's spatial response ($R(x, y)$) and the field distribution of the incident Gaussian beam ($I(x, y)$) from the source, expressed as

$$S(x, y) = R(x, y) * I(x, y) \tag{8}$$

The field distribution of the Gaussian beam can be modeled by knife-edge technique after calculating the beam waist size at the focus plane [134]. The effective area as the detector's

TABLE 4. 2D material-based THz detectors measurements comparison.

Detector type	Frequency (THz)	Antenna	Responsivity (V/W)	NEP (pW/$\sqrt{Hz}$)	THz Optical Measurements		Pixel	Ref
					P_{IN} calculation	A_{EFF} method		
Graphene FET	0.6	Bowtie + lens	14	515	C	VI	Single	[146]
Graphene Thermocouple	2.52	-	715	16	C	III	Single	[95]
Graphene FET	1.9	Double-patch + lens	4.9	1.7 nW	C	VI	Single	[152]
Graphene FET	0.325	log-periodic	0.25	80 nW	C	IV	Single	[129]
Graphene Photodetector	2	Bowtie	34 (μA/W)	150 nW	n/a	III	Single	[123]
Graphene FET	0.4	Bowtie + lens	74	130	C	VI	Single	[149]
Graphene Bolometer	2	Dipole	2 (mA/W)	-	C	III	Array	[100]
Graphene FET	0.487	Bowtie + lens	2	3 nW	C	VI	Single	[150]
Graphene FET	0.13	Log-spiral + lens	20	600	C	VI	Single	[156]
Graphene Photodetector	0.1	Spiral	28	350	C	III	Single	[119]
Graphene FET	0.14	Log-periodic	600	100	C	III	Single	[124]
BP FET	3.4	Bowtie	3	7 nW	n/a	IV	Single	[130]
Graphene Photodetector	2.5	Dipole	105	80	C	IV	Single	[131]
Graphene FET	0.3	Bowtie	70	0.06	C	VI	Array	[154]
Graphene Photodetector	3	Bowtie	180	18	C	IV	Single	[132]
Graphene Photodetector	2.52	LER microstructure	0.364	13.1 nW	n/a	III	Single	[125]
Graphene FET	0.3	Bowtie	1.8k	24	C	VI	Single	[157]
BP Photodetector	0.12 0.29	Bowtie	297 135	58 138	C	IV	Single	[133]
Graphene FET	0.13	Bowtie + lens	3k	0.2	C	VI	Single	[158]
Graphene/NiTeSe Photodetector	0.12 0.3	Bowtie	1.22 (A/W) 19 (mA/W)	18 pW 1.17 nW	C	III	Single	[120]
MAPbI3/PEDOT: PSS Photodetector	2.52	-	1 (μA/W)	3.3 nW	C	III	Single	[101]
Perovskite photodetector	2.52	-	0.321 (A/W)	300	C	III	Single	[121]

spatial response is then obtained using the deconvolution method by the Richardson-Lucy algorithm [135]. Fig. 9 displays the 3-D pattern of the field distribution, radiation beam, and detector's spatial response after deconvolution, as reported by Mao et al. [136]. This method is arguably the most accurate in determining the effective area of a detector because the beam area is characterized by the detector under test, thus including the contribution from the interfering structure such as the read-out circuit which is difficult to be predicted in a sole antenna measurement. Furthermore, it also gives additional information on the shape of the effective area. The accuracy of this method is dependent on the resolution of the 2-D scan, where a smaller step size would eventually produce a high-precision measurement dataset. However, the required long time for scanning the radiation beam and further processing processes have limited the reported works with this method [136], [137], [138].

6) NO AREA DEFINED

This method is primarily used as a direct comparison to the commercially available detectors, such as pyroelectric, Golay cells, bolometers, or thermopiles. Compared to the previous methods, the detector performance is optimized according to the total power of the focused THz beam, which is broadly used in the applications requiring a point-to-point measurement configuration, such as imaging systems [139], [140], [141], [142], [143], [144]. A large detector area beyond the diffraction-limit at 300 GHz is used to calculate the responsivity, and then a comparison is made to the one from the power meter without taking any normalization area [145]. Other works report the detector measurement referring to the in-situ power at the position of the detector. Thus, the responsivity can be taken as the lower limit without compensating the losses from the optical components [146], [147], [148], [149], [150], [151], [152], [153], [154], [155]. However, a more moderate measurement is also reported in which the total power measured by the reference detector includes the attenuation from the cryostat optical window, silicon lens transmission coefficient, antenna radiation efficiency, and additional losses caused by the probing mechanism [156], [157], [158], [159], [160], [161].

TABLE 5. Metallic and other thermal-based THz detectors measurements comparison.

Detector type	Frequency (THz)	Antenna	Responsivity (V/W)	NEP (pW/$\sqrt{Hz}$)	THz Optical Measurements		Pixel	Ref
					P_{IN} calculation	A_{EFF} method		
YBCO Bolometer	0.4	Log-spiral + lens	45	50	C	VI	Single	[159]
Al CEB	0.33	Twin-slot antenna	10^{10}	10^{-18} W/$\sqrt{Hz}$	A	VI	Single	[84]
Nb_5N_6 Bolometer	0.28	Dipole	480	-	C	V	Single	[136]
VOx Bolometer	2.5	Metasurface absorber	60k	37	C	III	Array	[96]
VOx Bolometer	2.5	Patch	331	123	C	III	Single	[122]
$LiTaO_3$ Pyroelectric	2.52	NiCr absorber	8.6k	1.5 nW	C	III	Array	[39]
PVDF Pyroelectric	0.3	Pyroelectric and metal thin film	0.351 (μA/W)	200 nW	C	VI	Single	[145]
VOx Bolometer	2.5	Patch	1.235k	87.4	C	III	Array	[102]
Pyroelectric film	0.14	Metasurface absorber	56k	2 nW	C	V	Array	[138]
NbN HEB	0.623	Log-spiral + lens	-	1.6	A	VI	Single	[85]
Nb_5N_6 Bolometer	0.335	Dipole	1.16k	-	C	VI	Array	[151]
NbN HEB	0.65	Log-spiral + lens	105	7	A	VI	Single	[83]
Nb_5N_6 Bolometer	0.64	Double-slot	312	-	C	III	Array	[114]
Nb_5N_6 Bolometer	0.64	Double-slot	113	44	C	II	Array	[112]
LSMO Bolometer	0.762	Log-periodic	0.9	-	C	V	Single	[137]
Cr/Au Bolometer	0.14	MEMS resonator	-	100	C	IV	Single	[128]
BiSb Thermocouple	0.812	Dipole	26	170	C	II	Single	[38]

V. DISCUSSION AND FUTURE DIRECTIONS

The summary of THz detector measurement methodology, including their two basic performance metrics, are presented in Table 2 for Si-based detectors, Table 3 for III-V materials-based detectors, Table 4 for the detector from the 2D material structure, and Table 5 for the metal-based THz detectors. Note that direct comparison between detectors might not be possible as the measurements include a wide range of input power and effective area measurement methodologies. The presented responsivities and NEPs were taken from the direct detection method, unless it specified otherwise.

Reference detector (Method C) is the mostly used method in determining the input radiation power from the THz source. More than 80% of the reviewed devices have used this method, with the distribution almost equal at any type of THz detector. The reference detector method offers the benefit of simpler operation and a more accurate estimation of radiated power rather than relying on the power information from the transmitter specification datasheet that might be degraded over time without proper re-calibration or attenuated by some random environmental noises. Furthermore, the calibration by reference detectors hypothetically includes the attenuation caused by atmospheric losses such as humidity, which is not covered by the classical microwave approach in the Friis transmission equation (Method B). As for the Planck's radiation law (Method A) is the least used method, which is normally used in THz detectors measured with a blackbody source radiation without any normalization area defined. Since the blackbody radiation covers a wide spectral range, the radiation intensity around the detector's center frequency is usually determined by the optical components, such as mesh filters, or the spectral matching information of the receiver antenna.

The data distribution in tables 2 - 5 also shows the significant spread of the normalization area method that can be applied to THz detector measurement. The most used method in determining the effective area is based on the physical area (Method III) and without any normalization area (Method VI). In the Si-based THz detectors shown in table 2, the pixel pitch size of array devices is used as the physical area to normalize the power. Moreover, in [113], the pixel size is reported to be almost similar to the area calculated based on the simulated directivity of the patch antenna, suggesting the effectiveness of using array size as it accounted for all the power incidents on the array. As for the other Si-based devices with single pixel report the detector area assuming the monolithically integrated antenna and FET detector area [93], [116]. For Method III in table 3 reports the active area of the photosensitive element to normalize the power. A novel approach is reported where an area of the gate electrode is used simultaneously as a metallic screen with a sub-wavelength aperture as the normalization area for InAs FET [126]. Method III in the graphene-based THz

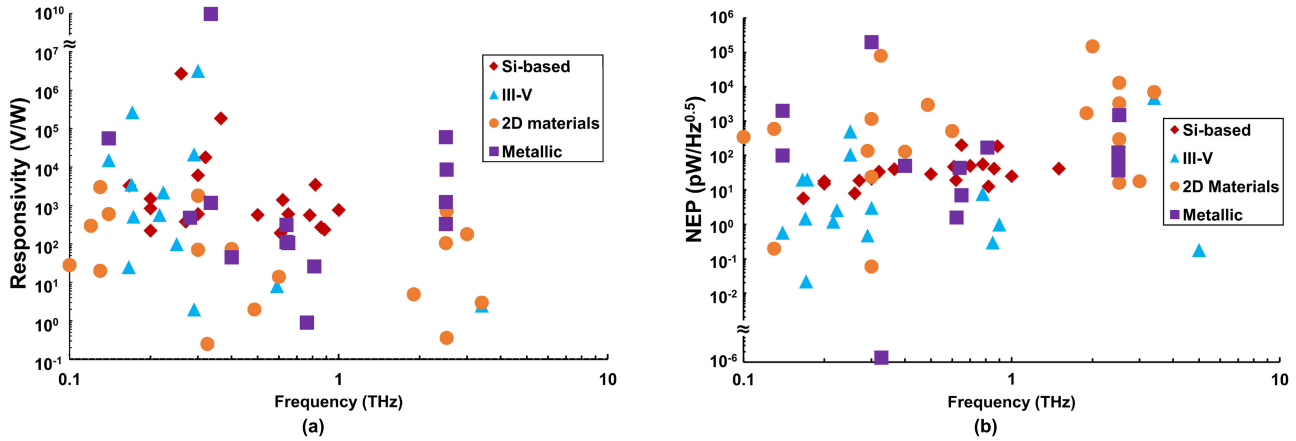

FIGURE 10. (a) Responsivity and (b) NEP distribution of the surveyed THz detectors as a function of THz frequency in different materials.

TABLE 6. Commercially available reference THz detectors and power meters.

Company	Model	Frequency	Aperture diameter	Power range	Ref
VDI	PM5B	0.075 - > 3 THz	1.25 x 2.5 mm	1 µW - 200 mW	[124]
Thomas Keating	Absolute Power Meter System	0.03 - > 3 THz	> 30 mm	200 mW (max)	[168]
Scientech, Inc	Vector H410	8 - 1200 THz	25.4 mm	5 W (max)	[169]
Keysight	W8486A	0.075 - 0.11 THz	1.25 x 2.5 mm	20 dBm (max)	[170]
Tydex	GC-1P	0.04 - 20 THz	6 mm	10 µW (max)	[171]
Gentec Electro-Optics	QS5-THZ-BL	0.1 - 30 THz	5 mm	60 µW (max)	[172]
Ophir	3A-P-THz	0.1 - 30 THz	12 mm	15µW - 3W	[173]

detector in table 4 refers to a fraction of the graphene area to the radiation beam spot to normalize the power. In comparison, the perovskite-based THz photodetectors use channel area and input power density calibrated by the power meter [101], [121]. As for metallic-based devices report the periodic area in arrayed structure and area of the micro bridge in a single pixel device for the power normalization based on the physical area.

From all the presented detectors in table 2 - 5, Method VI is mostly used in the III-V-materials-based THz detectors. Other types of THz detectors also show a similar method, implying the optical responsivity values as the lower bound (extrinsic) from the *in-situ* power calibrated by the reference detectors or power meters. In this manner, no radiation beam spot information nor device sizes are used to normalize the power. However, some reports suggest the optical losses by windows, lenses, or reflection loss by the antenna as accountable measurement quantity to reduce the radiated power, hence the optical responsivity can be comparable to the ones with the normalized power.

The devices fabricated using III-V, 2D, and metallic materials have a notable spread of effective area methods. Deconvolution-based normalization area (Method V) is the least used method and is only found in metallic-based devices, while the diffraction-limited area is found in the 2D-material detectors.

In addition to the results presented on the tables, the responsivity and NEP plots against THz frequency are given in Fig. 10. The NEP performance is more important from the detector system point of view compared to the responsivity, since NEP involves more experimental data in the measurements, while the responsivity characterizes the detector partially [162]. As shown, the spread of performance is large in both responsivity and NEP. However, smaller fluctuations could be found in Si-based detectors. The state-of-the-art fabrication technology advantage in CMOS allows for easy integration of detector with readout circuitry and other components, hence the determination of detector area by its physical or pixel size can be taken more accurate with less complexity compared to the other materials such as 2D materials, metallic, and III-V based detectors.

It is expected that THz applications require an accurate detector measurement to produce high sensitivity and low noise performance. Thus, considerable attention is needed when characterizing the detector system. Here we list the future directions as guidance for the THz researcher in the development of detectors.

A. SELECTION OF METHODOLOGY

As shown in the summary tables, different methodologies have been used by recent THz detectors in determining the input radiation power as well as the effective area. The selection of methods is, therefore, essential. In terms of input power measurement, a reference detector is highly anticipated as the method to calibrate the input power or radiation intensity impinged to the detector. This method offers flexibility as well as a degree of freedom compared to the

classical approach from the microwave domain by using the Friis transmission equation which requires an exact transmitter antenna and power transmitted by the THz source specification according to the provided information in the datasheet. Moreover, a pure Friis transmission method does not take into account specific setup losses. A combination of the Friis transmission method with the transmitted power calibrated by an external detector could also be considered. To give more perspective to the reader, we review some of the commercially available power meters for THz frequency bands and summarize them in Table 6. The reviewed devices are capable of measuring a wide THz spectral range from sub-mm wave to the far IR region with some examples of the important capabilities pointed out, such as aperture diameter and maximum readable power. In addition, THz detector measurement with a blackbody source can be chosen when the ultra-broadband detection performance is required, which is hardly covered by some electronic- or laser-based radiation sources.

B. OPTICAL LOSSES CONTRIBUTION

The optical performance quantities should be calculated with the inclusion of the optical losses involved in a measurement system. Measurement of radiation power by reference detector gives the estimated power at the detector location. Thus, one can expect the actual power impinged to the detector if it is measured after all optical elements (OAP mirrors, attenuators, etc.) placed in between the source and reference detector. However, other loss contributions still need to be considered, particularly from the elements attached or monolithically integrated with the detector. A silicon lens typically has an attenuation factor of 0.3 due to the reflection and surface wave losses. Improvement of antenna efficiency by eliminating the surface wave losses based on the quasi-optical configuration concept can be adopted using an extended hemispherical silicon lens or an antireflection coating [163].

THz measurements performed using a variable temperature optical cryostat allows for higher sensitivity performance due to suppression of the atmospheric losses such as high temperature and humidity surrounding the detector. The electromagnetic radiation is coupled to the detector through a window, which is commonly equipped with polyethylene material as a focusing mechanism. A correction of the incident power should be applied to account for losses occurring in the cryostat window. A high-density polyethylene (HDPE) window has typical transmittance of 0.9 at the low THz frequencies below 1 THz, and further decreases as the frequency increases [164]. However, the transmittance could be varied with the window thickness.

C. ANTENNA EFFICIENCY FACTOR

The efficiency factor from the antenna is another issue when determining the overall performance of an antenna-coupled detector. The first one is the coupling efficiency of the antenna pattern to the incident far-field pattern, which depends on the antenna (and lens) geometry. If Gaussian-distributed field radiation patterns are measured, one can refer to the Gaussian beam coupling efficiency (Gaussicity). A larger lens radius could achieve a higher directivity performance in a lens-coupled antenna design. However, this modification generally results in a Gaussicity decrease. A proper lens design is necessary to provide the highest Gaussicity while maintaining good antenna directivity [165].

A good matching between antenna and load impedances is necessary to reduce the reflection loss. For this reason, the antenna design should antenna targeted at the corresponding complex conjugate of the detector input impedance. A classic Smith chart method could be applied to plot the impedance circles of equal matching efficiency around the complex conjugate of a detector at the desired frequency. In a rectifying detector, one can apply the gate-source input impedance of the MOS transistor. Thus, the design criteria for the antenna impedance should be chosen with the highest matching efficiency.

Last but not least, additional losses included in the antenna are related to the polarization. The misalignment between the receiving and transmitting antenna electric field direction could lead to polarization-dependent loss. In the case of different polarization between receiving and transmitting antenna (e.g., elliptically polarized spiral antenna versus the linearly polarized horn antenna), an additional loss coupling factor could be further included.

VI. CONCLUSION

In this paper, we have surveyed methods involved in a THz detector measurement. The necessity of proper THz detector measurement has been discussed. A review of THz detector classification is presented based on multiple approaches. A detailed discussion on different radiation input power measurements is covered, along with the selection of effective area for the input power normalization. Our review suggest the deconvolution as the most reliable and accurate method to determine the detector's efective area since the scanned area includes the contribution from the interfering structure such as the read-out circuit thus systematic information on the shape of the effective area can be given. Furthermore, a comparison of different measurement methodologies available in recent THz detector researches is presented based on the detector's material. Si-based detectors show the less deviated range of performance compared to the other surveyed materials, thanks to the state-of-the-art advantage in CMOS technology for the precise determination of detector area with less complexity. Moreover, a review of the recently available THz power meters is given as guidance for the reader in selecting the proper input power calibration by a reference device. In the end, we have pointed the selection of input power and effective area measurement methods, optical losses contribution from the elements involved during measurements, and antenna efficiency factor as the future directions on the THz detector measurements.

REFERENCES

[1] J. Laufs, H. Borrion, and B. Bradford, "Security and the smart city: A systematic review," *Sustain. Cities Soc.*, vol. 55, Apr. 2020, Art. no. 102023, doi: 10.1016/j.scs.2020.102023.

[2] A. Rawson, "Recent advances in terahertz time-domain spectroscopy and imaging techniques for automation in agriculture and food sector," *Food Anal. Methods*, vol. 15, no. 2, pp. 498–526, Feb. 2022, doi: 10.1007/s12161-021-02132-y.

[3] D. Samanta, M. P. Karthikeyan, D. Agarwal, A. Biswas, A. Acharyya, and A. Banerjee, "Trends in terahertz biomedical applications," in *Generation, Detection and Processing of Terahertz Signals*. Singapore: Springer, 2022, pp. 285–299, doi: 10.1007/978-981-16-4947-9_19.

[4] Z. Chen, C. Han, Y. Wu, L. Li, C. Huang, Z. Zhang, G. Wang, and W. Tong, "Terahertz wireless communications for 2030 and beyond: A cutting-edge frontier," *IEEE Commun. Mag.*, vol. 59, no. 11, pp. 66–72, Nov. 2021, doi: 10.1109/MCOM.011.2100195.

[5] J. Kokkoniemi, J. Lehtomäki, K. Umebayashi, and M. Juntti, "Frequency and time domain channel models for nanonetworks in terahertz band," *IEEE Trans. Antennas Propag.*, vol. 63, no. 2, pp. 678–691, Feb. 2015, doi: 10.1109/TAP.2014.2373371.

[6] J. Li and J. Li, "Terahertz (THz) generator and detection," *Electr. Sci. Eng.*, vol. 2, no. 1, pp. 1–10, Apr. 2020, doi: 10.30564/ese.v2i1.1777.

[7] Z. Wu, K. Umebayashi, J. Lehtomakiy, and N. Zorba, "Device-to-device communications at the terahertz band: Open challenges for realistic implementation," *IEEE Commun. Standards Mag.*, early access, Dec. 12, 2022, doi: 10.1109/MCOMSTD.0001.2100077.

[8] J. E. Martin, N. P. Fox, and P. J. Key, "A cryogenic radiometer for absolute radiometric measurements," *Metrologia*, vol. 21, no. 3, pp. 147–155, Jan. 1985, doi: 10.1088/0026-1394/21/3/007.

[9] K. Ikamas, D. Čibiraitė, A. Lisauskas, M. Bauer, V. Krozer, and H. G. Roskos, "Broadband terahertz power detectors based on 90-nm silicon CMOS transistors with flat responsivity up to 2.2 THz," *IEEE Electron Device Lett.*, vol. 39, no. 9, pp. 1413–1416, Sep. 2018, doi: 10.1109/LED.2018.2859300.

[10] M. Bauer, A. R. Serguei A. Chevtchenko, K. Y. Osipov, D. Cibiraite, S. Pralgauskaite, and K. Ikamas, "A high-sensitivity AlGaN/GaN HEMT terahertz detector with integrated broadband bow-tie antenna," *IEEE Trans. THz Sci. Technol.*, vol. 9, no. 4, pp. 430–444, Jul. 2019, doi: 10.1109/TTHZ.2019.2917782.

[11] J. Zdanevicius, D. Cibiraite, K. Ikamas, M. Bauer, J. Matukas, A. Lisauskas, H. Richter, T. Hagelschuer, V. Krozer, H.-W. Hubers, and H. G. Roskos, "Field-effect transistor based detectors for power monitoring of THz quantum cascade lasers," *IEEE Trans. THz Sci. Technol.*, vol. 8, no. 6, pp. 613–621, Nov. 2018, doi: 10.1109/TTHZ.2018.2871360.

[12] A. G. Paulish, A. V. Gusachenko, A. O. Morozov, K. V. Dorozhkin, V. I. Suslyaev, V. A. Golyashov, O. V. Minin, and I. V. Minin, "Characterization of tetraaminediphenyl-based pyroelectric detector from visible to millimeter wave ranges," *Opt. Eng.*, vol. 59, no. 6, p. 1, Dec. 2019, doi: 10.1117/1.OE.59.6.061612.

[13] B. S. Karasik, A. V. Sergeev, and D. E. Prober, "Nanobolometers for THz photon detection," *IEEE Trans. THz Sci. Technol.*, vol. 1, no. 1, pp. 97–111, Sep. 2011, doi: 10.1109/TTHZ.2011.2159560.

[14] Z. Popovic and E. N. Grossman, "THz metrology and instrumentation," *IEEE Trans. THz Sci. Technol.*, vol. 1, no. 1, pp. 133–144, Sep. 2011, doi: 10.1109/TTHZ.2011.2159553.

[15] T. Otsuji, "Trends in the research of modern terahertz detectors: Plasmon detectors," *IEEE Trans. THz Sci. Technol.*, vol. 5, no. 6, pp. 1110–1120, Nov. 2015.

[16] J. Marczewski, D. Coquillat, W. Knap, C. Kolacinski, P. Kopyt, K. Kucharski, J. Lusakowski, D. Obrebski, D. Tomaszewski, D. Yavorskiy, P. Zagrajek, R. Ryniec, and N. Palka, "THz detectors based on Si-CMOS technology field effect transistors—Advantages, limitations and perspectives for THz imaging and spectroscopy," *Opto-Electron. Rev.*, vol. 26, no. 4, pp. 261–269, Dec. 2018, doi: 10.1016/j.opelre.2018.08.002.

[17] F. Sizov, "Terahertz radiation detectors: The state-of-the-art," *Semicond. Sci. Technol.*, vol. 33, no. 12, Dec. 2018, Art. no. 123001, doi: 10.1088/1361-6641/aae473.

[18] R. Bogue, "Sensing with terahertz radiation: A review of recent progress," *Sensor Rev.*, vol. 38, no. 2, pp. 216–222, Mar. 2018, doi: 10.1108/SR-10-2017-0221.

[19] R. A. Lewis, "A review of terahertz detectors," *J. Phys. D, Appl. Phys.*, vol. 52, no. 43, Oct. 2019, Art. no. 433001, doi: 10.1088/1361-6463/ab31d5.

[20] S. R. Kasjoo, M. B. M. Mokhar, N. F. Zakaria, and N. J. Juhari, "A brief overview of detectors used for terahertz imaging systems," in *Proc. AIP Conf.*, 2020, Art. no. 020020, doi: 10.1063/1.5142112.

[21] J. Xie, W. Ye, L. Zhou, X. Guo, X. Zang, L. Chen, and Y. Zhu, "A review on terahertz technologies accelerated by silicon photonics," *Nanomaterials*, vol. 11, no. 7, p. 1646, Jun. 2021, doi: 10.3390/nano11071646.

[22] E. Javadi, D. B. But, K. Ikamas, J. Zdanevičius, W. Knap, and A. Lisauskas, "Sensitivity of field-effect transistor-based terahertz detectors," *Sensors*, vol. 21, no. 9, p. 2909, Apr. 2021, doi: 10.3390/s21092909.

[23] X. Lu, S. Venkatesh, and H. Saeidi, "A review on applications of integrated terahertz systems," *China Commun.*, vol. 18, no. 5, pp. 175–201, May 2021, doi: 10.23919/JCC.2021.05.011.

[24] J. Wang, M. Naftaly, and E. Wasige, "An overview of terahertz imaging with resonant tunneling diodes," *Appl. Sci.*, vol. 12, no. 8, p. 3822, Apr. 2022, doi: 10.3390/app12083822.

[25] M. C. Teich, "The physics of heterodyne detection in the far-infrared: Transition from electric-field to photon-absorption detection in a simple system," in *Proc. NASA Conf. Publication*. Hampton, VI, USA: NASA Langley Res. Center, Aug. 1980.

[26] F. Ellinger, D. Fritsche, G. Tretter, J. D. Leufker, U. Yodprasit, and C. Carta, "Review of millimeter-wave integrated circuits with low power consumption for high speed wireless communications," *Frequenz*, vol. 71, nos. 1–2, pp. 1–9, Jan. 2017, doi: 10.1515/freq-2016-0119.

[27] D. Yoon, J. Kim, J. Yun, M. Kaynak, B. Tillack, and J.-S. Rieh, "300-GHz direct and heterodyne active imagers based on 0.13-μm SiGe HBT technology," *IEEE Trans. THz Sci. Technol.*, vol. 7, no. 5, pp. 536–545, Sep. 2017, doi: 10.1109/TTHZ.2017.2715419.

[28] M. A. Kinch, "Fundamental physics of infrared detector materials," *J. Electron. Mater.*, vol. 29, no. 6, pp. 809–817, Jun. 2000, doi: 10.1007/s11664-000-0229-7.

[29] A. Rogalski, "HgCdTe infrared detector material: History, status and outlook," *Rep. Prog. Phys.*, vol. 68, no. 10, pp. 2267–2336, 2005, doi: 10.1088/0034-4885/68/10/R01.

[30] T. Wada, Y. Arai, S. Baba, M. Hanaoka, Y. Hattori, H. Ikeda, H. Kaneda, C. Kochi, A. Miyachi, K. Nagase, H. Nakaya, M. Ohno, S. Oyabu, T. Suzuki, S. Ukai, K. Watanabe, and K. Yamamoto, "Development for germanium blocked impurity band far-infrared image sensors with fully-depleted silicon-on-insulator CMOS readout integrated circuit," *J. Low Temp. Phys.*, vol. 184, nos. 1–2, pp. 217–224, Jul. 2016, doi: 10.1007/s10909-016-1522-z.

[31] M. Hanaoka, H. Kaneda, S. Oyabu, M. Yamagishi, Y. Hattori, S. Ukai, and K. Shichi, "Development of blocked-impurity-band-type Ge detectors fabricated with the surface-activated wafer bonding method for far-infrared astronomy," *J. Low Temp. Phys.*, vol. 184, nos. 1–2, pp. 225–230, Jul. 2016, doi: 10.1007/s10909-016-1484-1.

[32] F. Wu, W. Tian, W. Y. Yan, J. Zhang, S. C. Sun, J. N. Dai, Y. Y. Fang, Z. H. Wu, and C. Q. Chen, "Terahertz intersubband transition in GaN/AlGaN step quantum well," *J. Appl. Phys.*, vol. 113, no. 15, Apr. 2013, Art. no. 154505, doi: 10.1063/1.4802496.

[33] M. Graf, G. Scalari, D. Hofstetter, J. Faist, H. Beere, E. Linfield, D. Ritchie, and G. Davies, "Terahertz range quantum well infrared photodetector," *Appl. Phys. Lett.*, vol. 84, no. 4, pp. 475–477, Jan. 2004, doi: 10.1063/1.1641165.

[34] A. Rogalski and F. Sizov, "Terahertz detectors and focal plane arrays," *Opto-Electron. Rev.*, vol. 19, no. 3, pp. 346–404, Jan. 2011, doi: 10.2478/s11772-011-0033-3.

[35] M. Jeannin, T. Bonazzi, D. Gacemi, A. Vasanelli, S. Suffit, L. Li, A. G. Davies, E. Linfield, C. Sirtori, and Y. Todorov, "High temperature metamaterial terahertz quantum detector," *Appl. Phys. Lett.*, vol. 117, no. 25, Dec. 2020, Art. no. 251102, doi: 10.1063/5.0033367.

[36] D. R. Denison, M. E. Knotts, M. E. McConney, and V. V. Tsukruk, "Experimental characterization of mm-wave detection by a micro-array of Golay cells," *Proc. SPIE*, vol. 7309, May 2009, Art. no. 73090J, doi: 10.1117/12.818387.

[37] F. Simoens and J. Meilhan, "Terahertz real-time imaging uncooled array based on antenna- and cavity-coupled bolometers," *Phil. Trans. Roy. Soc. A, Math., Phys. Eng. Sci.*, vol. 372, no. 2012, Mar. 2014, Art. no. 20130111, doi: 10.1098/rsta.2013.0111.

[38] A. K. Huhn, G. Spickermann, A. Ihring, U. Schinkel, H.-G. Meyer, and P. H. Bolívar, "Uncooled antenna-coupled terahertz detectors with 22 μs response time based on BiSb/Sb thermocouples," *Appl. Phys. Lett.*, vol. 102, no. 12, Mar. 2013, Art. no. 121102, doi: 10.1063/1.4798369.

[39] W. Li, J. Wang, J. Gou, Z. Huang, and Y. Jiang, "Fabrication and characterization of linear terahertz detector arrays based on lithium tantalate crystal," *J. Infr., Millim., THz Waves*, vol. 36, no. 1, pp. 42–48, Jan. 2015, doi: 10.1007/s10762-014-0115-7.

[40] W. Miao, F. Li, Q. Luo, Q. Wang, J. Zhong, Z. Wang, K. Zhou, Y. Ren, W. Zhang, J. Li, S. Shi, C. Yu, Z. He, Q. Liu, and Z. Feng, "A terahertz detector based on superconductor-graphene-superconductor Josephson junction," *Carbon*, vol. 202, pp. 112–117, Jan. 2023, doi: 10.1016/j.carbon.2022.11.040.

[41] V. G. Bozhkov, "Semiconductor detectors, mixers, and frequency multipliers for the terahertz band," *Radiophys. Quantum Electron.*, vol. 46, no. 8/9, pp. 631–656, Aug. 2003, doi: 10.1023/B:RAQE.0000024993.40125.2b.

[42] T. W. Crowe, R. J. Mattauch, H. P. Roser, W. L. Bishop, W. C. B. Peatman, and X. Liu, "GaAs Schottky diodes for THz mixing applications," *Proc. IEEE*, vol. 80, no. 11, pp. 1827–1841, Nov. 1992, doi: 10.1109/5.175258.

[43] D. W. Park, E. S. Lee, J.-W. Park, H.-S. Kim, I.-M. Lee, and K. H. Park, "InGaAs Schottky barrier diode array detectors integrated with broadband antenna," *Proc. SPIE*, vol. 10103, Apr. 2017, Art. no. 101030F, doi: 10.1117/12.2251621.

[44] D. Schoenherr, C. Bleasdale, T. Goebel, C. Sydlo, H. L. Hartnagel, R. Lewis, and P. Meissner, "Extremely broadband characterization of a Schottky diode based THz detector," in *Proc. 35th Int. Conf. Infr., Millim., THz Waves*, Sep. 2010, pp. 1–2, doi: 10.1109/ICIMW.2010.5613008.

[45] E. R. Brown, A. C. Young, J. Zimmerman, H. Kazerni, and A. C. Gossard, "Advances in Schottky rectifier performance," *IEEE Microw. Mag.*, vol. 8, no. 3, pp. 54–59, Jun. 2007, doi: 10.1109/MMW.2007.365059.

[46] M. I. Dyakonov and M. S. Shur, "Plasma wave electronics: Novel terahertz devices using two dimensional electron fluid," *IEEE Trans. Electron Devices*, vol. 43, no. 10, pp. 1640–1645, Oct. 1996, doi: 10.1109/16.536809.

[47] X. Deng, M. Simanullang, and Y. Kawano, "Ge-core/a-Si-shell nanowire-based field-effect transistor for sensitive terahertz detection," *Photonics*, vol. 5, no. 2, p. 13, May 2018, doi: 10.3390/photonics5020013.

[48] W. Knap, M. Dyakonov, D. Coquillat, F. Teppe, N. Dyakonova, J. Łusakowski, K. Karpierz, M. Sakowicz, G. Valusis, D. Seliuta, I. Kasalynas, A. Fatimy, Y. M. Meziani, and T. Otsuji, "Field effect transistors for terahertz detection: Physics and first imaging applications," *J. Infr., Millim., THz Waves*, vol. 30, pp. 1319–1337, Aug. 2009, doi: 10.1007/s10762-009-9564-9.

[49] Z. Huang, Z. Li, H. Dong, F. Yang, W. Yan, and X. Wang, "Novel broadband slot-spiral antenna for terahertz applications," *Photonics*, vol. 8, no. 4, p. 123, Apr. 2021, doi: 10.3390/photonics8040123.

[50] S. Boppel, A. Lisauskas, M. Mundt, D. Seliuta, L. Minkevicius, I. Kasalynas, and G. Valusis, "CMOS integrated antenna-coupled field-effect transistors for the detection of radiation from 0.2 to 4.3 THz," *IEEE Trans. Microw. Theory Techn.*, vol. 60, no. 12, pp. 3834–3843, Dec. 2012, doi: 10.1109/TMTT.2012.2221732.

[51] P. Kopyt, J. Marczewski, K. Kucharski, J. Lusakowski, and W. K. Gwarek, "Planar antennas for THz radiation detector based on a MOSFET," in *Proc. Int. Conf. Infr., Millim., THz Waves*, Oct. 2011, pp. 1–2, doi: 10.1109/irmmw-THZ.2011.6105129.

[52] U. R. Pfeiffer, E. Ojefors, A. Lisauskas, D. Glaab, F. Voltolina, V. M. F. Nzogang, P. H. Bolivar, and H. G. Roskos, "A CMOS focal-plane array for terahertz imaging," in *Proc. 33rd Int. Conf. Infr., Millim. THz Waves*, Sep. 2008, pp. 1–3, doi: 10.1109/ICIMW.2008.4665429.

[53] A. Jooshesh, F. Fesharaki, V. Bahrami-Yekta, M. Mahtab, T. Tiedje, T. E. Darcie, and R. Gordon, "Plasmon-enhanced LT-GaAs/AlAs heterostructure photoconductive antennas for sub-bandgap terahertz generation," *Opt. Exp.*, vol. 25, no. 18, p. 22140, Sep. 2017, doi: 10.1364/OE.25.022140.

[54] A. E. Yachmenev, S. S. Pushkarev, R. R. Reznik, R. A. Khabibullin, and D. S. Ponomarev, "Arsenides-and related III–V materials-based multilayered structures for terahertz applications: Various designs and growth technology," *Prog. Crystal Growth Characterization Mater.*, vol. 66, no. 2, May 2020, Art. no. 100485, doi: 10.1016/j.pcrysgrow.2020.100485.

[55] T. Tanigawa, T. Onishi, S. Takigawa, and T. Otsuji, "Enhanced responsivity in a novel AlGaN/GaN plasmon-resonant terahertz detector using gate-dipole antenna with parasitic elements," in *Proc. 68th Device Res. Conf.*, Jun. 2010, pp. 167–168, doi: 10.1109/DRC.2010.5551895.

[56] A. El Moutaouakil, T. Suemitsu, T. Otsuji, H. Videlier, S. Boubanga-Tombet, D. Coquillat, and W. Knap, "Device loading effect on nonresonant detection of terahertz radiation in dual grating gate plasmon-resonant structure using InGaP/InGaAs/GaAs material systems," *Phys. Status Solidi C*, vol. 8, no. 2, pp. 346–348, Feb. 2011, doi: 10.1002/pssc.201000569.

[57] N. T. Yardimci, D. Turan, S. Cakmakyapan, and M. Jarrahi, "A high-responsivity and broadband photoconductive terahertz detector based on a plasmonic nanocavity," *Appl. Phys. Lett.*, vol. 113, no. 25, Dec. 2018, Art. no. 251102, doi: 10.1063/1.5066243.

[58] A. K. Geim and K. S. Novoselov, "The rise of graphene," *Nature Mater.*, vol. 6, pp. 183–191, Mar. 2007, doi: 10.1038/nmat1849.

[59] K. S. Novoselov, A. K. Geim, S. V. Morozov, D. Jiang, Y. Zhang, S. V. Dubonos, I. V. Grigorieva, and A. A. Firsov, "Electric field effect in atomically thin carbon films," *Science*, vol. 306, no. 5696, pp. 666–669, 2004, doi: 10.1126/science.1102896.

[60] C. Liu, L. Du, W. Tang, D. Wei, J. Li, L. Wang, G. Chen, X. Chen, and W. Lu, "Towards sensitive terahertz detection via thermoelectric manipulation using graphene transistors," *NPG Asia Mater.*, vol. 10, no. 4, pp. 318–327, Apr. 2018, doi: 10.1038/s41427-018-0032-7.

[61] V. Ryzhii, T. Otsuji, M. Ryzhii, N. Ryabova, S. O. Yurchenko, V. Mitin, and M. S. Shur, "Graphene terahertz uncooled bolometers," *J. Phys. D, Appl. Phys.*, vol. 46, no. 6, Feb. 2013, Art. no. 065102, doi: 10.1088/0022-3727/46/6/065102.

[62] S. Cakmakyapan, P. K. Lu, A. Navabi, and M. Jarrahi, "Gold-patched graphene nano-stripes for high-responsivity and ultrafast photodetection from the visible to infrared regime," *Light, Sci. Appl.*, vol. 7, no. 1, p. 20, Jun. 2018, doi: 10.1038/s41377-018-0020-2.

[63] Z. Xie, J. Wang, and J. T. W. Yeow, "Doped polyaniline/graphene composites for photothermoelectric detectors," *ACS Appl. Nano Mater.*, vol. 5, no. 6, pp. 7967–7973, Jun. 2022, doi: 10.1021/acsanm.2c01039.

[64] W. Lu, J. Ning, Y. Zhou, J. Dong, C. Yan, X. Shen, C. Zhang, D. Wang, J. Zhang, and Y. Hao, "High-responsivity molybdenum diselenide photodetector with dirac electrodes," *J. Alloys Compounds*, vol. 865, Jun. 2021, Art. no. 158939, doi: 10.1016/j.jallcom.2021.158939.

[65] X. Chen, J. S. Ponraj, D. Fan, and H. Zhang, "An overview of the optical properties and applications of black phosphorus," *Nanoscale*, vol. 12, no. 6, pp. 3513–3534, Feb. 2020, doi: 10.1039/C9NR09122J.

[66] L. Britnell, R. M. Ribeiro, A. Eckmann, R. Jalil, B. D. Belle, A. Mishchenko, and Y.-J. Kim, "Strong light-matter interactions in heterostructures of atomically thin films," *Science*, vol. 340, no. 6138, pp. 1311–1314, Jun. 2013, doi: 10.1126/science.1235547.

[67] M. Long, P. Wang, H. Fang, and W. Hu, "Progress, challenges, and opportunities for 2D material based photodetectors," *Adv. Funct. Mater.*, vol. 29, no. 19, May 2019, Art. no. 1803807, doi: 10.1002/adfm.201803807.

[68] Y. Wang, W. Wu, and Z. Zhao, "Recent progress and remaining challenges of 2D material-based terahertz detectors," *Infr. Phys. Technol.*, vol. 102, Nov. 2019, Art. no. 103024, doi: 10.1016/j.infrared.2019.103024.

[69] A. Rogalski, M. Kopytko, and P. Martyniuk, "Two-dimensional infrared and terahertz detectors: Outlook and status," *Appl. Phys. Rev.*, vol. 6, no. 2, Jun. 2019, Art. no. 021316, doi: 10.1063/1.5088578.

[70] H. Xu, A. Ren, J. Wu, and Z. Wang, "Recent advances in 2D MXenes for photodetection," *Adv. Funct. Mater.*, vol. 30, no. 24, Jun. 2020, Art. no. 2000907, doi: 10.1002/adfm.202000907.

[71] Y. I. Jhon, M. Seo, and Y. M. Jhon, "First-principles study of a MXene terahertz detector," *Nanoscale*, vol. 10, no. 1, pp. 69–75, 2018, doi: 10.1039/C7NR05351G.

[72] V. S. Sivasankarapillai, T. S. K. Sharma, K.-Y. Hwa, S. M. Wabaidur, S. Angaiah, and R. Dhanusuraman, "MXene based sensing materials: Current status and future perspectives," *ES Energy Environ.*, vol. 15, pp. 4–14, Jan. 2022, doi: 10.30919/esee8c618.

[73] I. Kašalynas, R. Venckevičius, L. Minkevičius, A. Sešek, F. Wahaia, V. Tamošiūnas, B. Voisiat, D. Seliuta, G. Valušis, A. Švigelj, and J. Trontelj, "Spectroscopic terahertz imaging at room temperature employing microbolometer terahertz sensors and its application to the study of carcinoma tissues," *Sensors*, vol. 16, no. 4, p. 432, Mar. 2016, doi: 10.3390/s16040432.

[74] A. Chakrabarty, M. A. Lindeman, B. Bumble, A. W. Kleinsasser, W. A. Holmes, and D. Cunnane, "Operation of YBCO kinetic-inductance bolometers for outer solar system missions," *Appl. Phys. Lett.*, vol. 114, no. 13, Apr. 2019, Art. no. 132601, doi: 10.1063/1.5089143.

[75] T. Quinten, Y. Lechaux, V. Pierron, J.-F. Lampin, C. Gunther, L. Mechin, M. Faucher, B. Walter, and B. Guillet, "Impedance measurements in $La_{0.7}Sr_{0.3}MnO_3$ thin films for uncooled THz bolometers," in *Proc. 47th Int. Conf. Infr., Millim. THz Waves*, Aug. 2022, pp. 1–2, doi: 10.1109/IRMMW-THz50927.2022.9896104.

[76] H. Shi, R. Su, T. Xu, X. Jia, L. Kang, X. Tu, J. Chen, and P. Wu, "The performance of suspended superconducting NbN hot electron bolometer with buffer layer," in *Proc. 47th Int. Conf. Infr., Millim. THz Waves*, Aug. 2022, pp. 1–2, doi: 10.1109/IRMMW-THz50927.2022.9895588.

[77] S. Ben Mbarek, S. Euphrasie, T. Baron, L. Thiery, P. Vairac, B. Cretin, J.-P. Guillet, and L. Chusseau, "Room temperature thermopile THz sensor," *Sens. Actuators A, Phys.*, vol. 193, pp. 155–160, Apr. 2013, doi: 10.1016/j.sna.2013.01.014.

[78] M. Aleksandrova, C. Jagtap, V. Kadam, S. Jadkar, G. Kolev, K. Denishev, and H. Pathan, "An overview of microelectronic infrared pyroelectric detector," *Engineered Sci.*, vol. 16, pp. 82–89, Jan. 2021, doi: 10.30919/es8d535.

[79] F. Sizov and A. Rogalski, "THz detectors," *Prog. Quantum Electron.*, vol. 34, no. 5, pp. 278–347, Sep. 2010, doi: 10.1016/j.pquantelec.2010.06.002.

[80] M. Perenzoni and D. J. Paul, *Physics and Applications of Terahertz Radiation*, vol. 173. Dordrecht, The Netherlands: Springer, 2014, doi: 10.1007/978-94-007-3837-9.

[81] A. Rogalski, *Infrared and Terahertz Detectors*, 3rd ed. Boca Raton, NJ, USA: CRC Press, 2019.

[82] D. Palaferri, Y. Todorov, Y. N. Chen, J. Madeo, A. Vasanelli, L. H. Li, A. G. Davies, E. H. Linfield, and C. Sirtori, "Patch antenna terahertz photodetectors," *Appl. Phys. Lett.*, vol. 106, no. 16, Apr. 2015, Art. no. 161102, doi: 10.1063/1.4918983.

[83] R. F. Su, Y. D. Zhang, X. Tu, X. Jia, L. Kang, B. B. Jin, J. Chen, and P. Wu, "Terahertz direct detectors based on superconducting hot electron bolometers with different biasing methods," *IEEE Trans. Appl. Supercond.*, vol. 29, no. 5, pp. 1–4, Aug. 2019, doi: 10.1109/TASC.2019.2906785.

[84] M. A. Tarasov, V. S. Edelman, A. B. Ermakov, S. Mahashabde, and L. S. Kuzmin, "Quantum efficiency of cold electron bolometer optical response," *IEEE Trans. THz Sci. Technol.*, vol. 5, no. 1, pp. 44–48, Jan. 2015, doi: 10.1109/TTHZ.2014.2379331.

[85] S. L. Jiang, X. F. Li, X. Q. Jia, L. Kang, B. B. Jin, W. W. Xu, J. Chen, and P. H. Wu, "Appropriate microwave frequency selection for biasing superconducting hot electron bolometers as terahertz direct detectors," *Supercond. Sci. Technol.*, vol. 30, no. 4, Apr. 2017, Art. no. 044004, doi: 10.1088/1361-6668/aa621b.

[86] H. Qiao, H. Liu, J. Mou, S. Liu, B. Wang, D. Guo, and X. Lv, "Compact terahertz detector based on lightweight 3D-printed lens packaging," *Electron. Lett.*, vol. 55, no. 14, pp. 796–797, Jul. 2019, doi: 10.1049/el.2019.1446.

[87] M. I. W. Khan, S. Kim, D.-W. Park, H.-J. Kim, S.-K. Han, and S.-G. Lee, "Nonlinear analysis of nonresonant THz response of MOSFET and implementation of a high-responsivity cross-coupled THz detector," *IEEE Trans. THz Sci. Technol.*, vol. 8, no. 1, pp. 108–120, Jan. 2018, doi: 10.1109/TTHZ.2017.2778499.

[88] R. A. Hadi, J. Grzyb, B. Heinemann, and U. R. Pfeiffer, "A terahertz detector array in a SiGe HBT technology," *IEEE J. Solid-State Circuits*, vol. 48, no. 9, pp. 2002–2010, Sep. 2013, doi: 10.1109/JSSC.2013.2265493.

[89] R. Han, Y. Zhang, Y. Kim, D. Y. Kim, H. Shichijo, and E. Afshari, "Active terahertz imaging using Schottky diodes in CMOS: Array and 860-GHz pixel," *IEEE J. Solid-State Circuits*, vol. 48, no. 10, pp. 2296–2308, Oct. 2013, doi: 10.1109/JSSC.2013.2269856.

[90] K. Sengupta, D. Seo, L. Yang, and A. Hajimiri, "Silicon integrated 280 GHz imaging chipset with 4 × 4 SiGe receiver array and CMOS source," *IEEE Trans. THz Sci. Technol.*, vol. 5, no. 3, pp. 427–437, May 2015, doi: 10.1109/TTHZ.2015.2414826.

[91] D. Y. Kim, S. Park, and R. Han, "Design and demonstration of 820-GHz array using diode-connected NMOS transistors in 130-nm CMOS for active imaging," *IEEE Trans. THz Sci. Technol.*, vol. 6, no. 2, pp. 306–317, Mar. 2016, doi: 10.1109/TTHZ.2015.2513061.

[92] J. Mou, Q. Xue, D. Guo, and X. Lv, "A THz detector chip with printed circular cavity as package and enhancement of antenna gain," *IEEE Trans. Antennas Propag.*, vol. 64, no. 4, pp. 1242–1249, Apr. 2016, doi: 10.1109/TAP.2016.2526068.

[93] M. W. Ryu, J. S. Lee, K. Park, W.-K. Park, S.-T. Han, and K. R. Kim, "Photoresponse enhancement of plasmonic terahertz wave detector based on asymmetric silicon MOSFETs with antenna integration," *Jpn. J. Appl. Phys.*, vol. 53, no. 4S, Apr. 2014, Art. no. 04EJ05, doi: 10.7567/JJAP.53.04EJ05.

[94] Y. Kurita, G. Ducournau, D. Coquillat, A. Satou, K. Kobayashi, S. B. Tombet, Y. M. Meziani, V. V. Popov, W. Knap, T. Suemitsu, and T. Otsuji, "Ultrahigh sensitive sub-terahertz detection by InP-based asymmetric dual-grating-gate high-electron-mobility transistors and their broadband characteristics," *Appl. Phys. Lett.*, vol. 104, no. 25, Jun. 2014, Art. no. 251114, doi: 10.1063/1.4885499.

[95] X. Cai, A. B. Sushkov, R. J. Suess, M. M. Jadidi, G. S. Jenkins, L. O. Nyakiti, and R. L. Myers-Ward, "Sensitive room-temperature terahertz detection via the photothermoelectric effect in graphene," *Nature Nanotechnol.*, vol. 9, pp. 814–819, Sep. 2014, doi: 10.1038/nnano.2014.182.

[96] I. E. Carranza, J. Grant, J. Gough, and D. R. S. Cumming, "Metamaterial-based terahertz imaging," *IEEE Trans. THz Sci. Technol.*, vol. 5, no. 6, pp. 892–901, Nov. 2015, doi: 10.1109/TTHZ.2015.2463673.

[97] Y. Qu, W. Zhou, J. Tong, N. Yao, X. Xu, T. Hu, Z. Huang, and J. Chu, "High sensitivity of room-temperature sub-terahertz photodetector based on $In_{0.53}Ga_{0.47}As$ material," *Appl. Phys. Exp.*, vol. 11, no. 11, Nov. 2018, Art. no. 112201, doi: 10.7567/APEX.11.112201.

[98] C. Wu, W. Zhou, N. Yao, X. Xu, Y. Qu, Z. Zhang, J. Wu, L. Jiang, Z. Huang, and J. Chu, "Silicon-based high sensitivity of room-temperature microwave and sub-terahertz detector," *Appl. Phys. Exp.*, vol. 12, no. 5, May 2019, Art. no. 052013, doi: 10.7567/1882-0786/ab14fc.

[99] J. Tong, Y. Qu, F. Suo, W. Zhou, Z. Huang, and D. H. Zhang, "Antenna-assisted subwavelength metal–InGaAs–metal structure for sensitive and direct photodetection of millimeter and terahertz waves," *Photon. Res.*, vol. 7, no. 1, p. 89, Jan. 2019, doi: 10.1364/PRJ.7.000089.

[100] R. Degl'Innocenti, L. Xiao, S. J. Kindness, V. S. Kamboj, B. Wei, P. Braeuninger-Weimer, K. Nakanishi, A. I. Aria, S. Hofmann, H. E. Beere, and D. A. Ritchie, "Bolometric detection of terahertz quantum cascade laser radiation with graphene-plasmonic antenna arrays," *J. Phys. D, Appl. Phys.*, vol. 50, no. 17, May 2017, Art. no. 174001, doi: 10.1088/1361-6463/aa64bf.

[101] Y. Li, Y. Zhang, T. Li, X. Tang, M. Li, Z. Chen, Q. Li, Q. Sheng, W. Shi, and J. Yao, "A fast response, self-powered and room temperature near infrared-terahertz photodetector based on a $MAPbI_3$/PEDOT:PSS composite," *J. Mater. Chem. C*, vol. 8, no. 35, pp. 12148–12154, Sep. 2020, doi: 10.1039/D0TC02399J.

[102] X. Zheng, Z. Wu, J. Gou, Z. Liu, J. Wang, J. Zheng, Z. Luo, W. Chen, L. Que, and Y. Jiang, "Enhancement of real-time THz imaging system based on 320 × 240 uncooled microbolometer detector," *J. Infr., Millim., THz Waves*, vol. 37, no. 10, pp. 965–976, Oct. 2016, doi: 10.1007/s10762-016-0287-4.

[103] A. Steiger, M. Kehrt, C. Monte, and R. Müller, "Traceable terahertz power measurement from 1 THz to 5 THz," *Opt. Exp.*, vol. 21, no. 12, p. 14466, Jun. 2013, doi: 10.1364/OE.21.014466.

[104] C. W. Berry, T. N. Yardimci, and M. Jarrahi, "Responsivity calibration of pyroelectric terahertz detectors," 2014, *arXiv:1412.6878*.

[105] C.-T. Tai and C. Pereira, "An approximate formula for calculating the directivity of an antenna," *IEEE Trans. Antennas Propag.*, vol. AP-24, no. 2, pp. 235–236, Mar. 1976, doi: 10.1109/TAP.1976.1141313.

[106] Z. Ahmad and K. K. O, "THz detection using p^+/n-well diodes fabricated in 45-nm CMOS," *IEEE Electron Device Lett.*, vol. 37, no. 7, pp. 823–826, Jul. 2016, doi: 10.1109/LED.2016.2573268.

[107] M. Khatib and M. Perenzoni, "Response optimization of antenna-coupled FET detectors for 0.85-to-1-THz imaging," *IEEE Microw. Wireless Compon. Lett.*, vol. 28, no. 10, pp. 903–905, Oct. 2018, doi: 10.1109/LMWC.2018.2860794.

[108] G. Karolyi, D. Gergelyi, and P. Foldesy, "Sub-THz sensor array with embedded signal processing in 90 nm CMOS technology," *IEEE Sensors J.*, vol. 14, no. 8, pp. 2432–2441, Aug. 2014, doi: 10.1109/JSEN.2013.2291316.

[109] C. Balanis, *Antenna Theory: Analysis and Design*, 4th ed. Hoboken, NJ, USA: Wiley, 2016, pp. 75–78.

[110] C.-H. Li and T.-Y. Chiu, "Single flip-chip packaged dielectric resonator antenna for CMOS terahertz antenna array gain enhancement," *IEEE Access*, vol. 7, pp. 7737–7746, 2019, doi: 10.1109/ACCESS.2018.2890678.

[111] J. Tong, F. Suo, T. Zhang, Z. Huang, J. Chu, and D. H. Zhang, "Plasmonic semiconductor nanogroove array enhanced broad spectral band millimetre and terahertz wave detection," *Light, Sci. Appl.*, vol. 10, no. 1, pp. 1–10, Mar. 2021, doi: 10.1038/s41377-021-00505-w.

[112] P. Xiao, X. Tu, C. Jiang, Z. Li, S. Zhou, D. Pan, Q. Zhao, X. Jia, L. Zhang, L. Kang, J. Chen, and P. Wu, "Planar double-slot antenna integrated into a Nb_5N_6 microbolometer THz detector," *Opt. Lett.*, vol. 45, no. 10, p. 2894, May 2020, doi: 10.1364/ol.388771.

[113] M. Uzunkol, O. D. Gurbuz, F. Golcuk, and G. M. Rebeiz, "A 0.32 THz SiGe 4×4 imaging array using high-efficiency on-chip antennas," *IEEE J. Solid-State Circuits*, vol. 48, no. 9, pp. 2056–2066, Sep. 2013, doi: 10.1109/JSSC.2013.2262739.

[114] P. Xiao, X. Tu, L. Kang, Z. Li, P. Chen, S. Zhou, X. Jia, J. Chen, and P. Wu, "Design of double-slot antennas for terahertz array detectors in flip chip packaging," *Opt. Exp.*, vol. 28, no. 6, p. 8783, Mar. 2020, doi: 10.1364/OE.389048.

[115] D. Coquillat, J. Marczewski, P. Kopyt, N. Dyakonova, B. Giffard, and W. Knap, "Improvement of terahertz field effect transistor detectors by substrate thinning and radiation losses reduction," *Opt. Exp.*, vol. 24, no. 1, p. 272, Jan. 2016, doi: 10.1364/OE.24.000272.

[116] M. W. Ryu, K. S. Kim, J. S. Lee, K. Park, J.-R. Yang, S.-T. Han, and K. R. Kim, "Performance enhancement of plasmonic sub-terahertz detector based on antenna integrated low-impedance silicon MOSFET," *IEEE Electron Device Lett.*, vol. 36, no. 3, pp. 220–222, Mar. 2015, doi: 10.1109/LED.2015.2394446.

[117] M. W. Ryu, J. S. Lee, K. S. Kim, K. Park, J.-R. Yang, S.-T. Han, and K. R. Kim, "High-performance plasmonic THz detector based on asymmetric FET with vertically integrated antenna in CMOS technology," *IEEE Trans. Electron Devices*, vol. 63, no. 4, pp. 1742–1748, Apr. 2016, doi: 10.1109/TED.2016.2526677.

[118] H. Hou, Z. Liu, J. Teng, T. Palacios, and S.-J. Chua, "A sub-terahertz broadband detector based on a GaN high-electron-mobility transistor with nanoantennas," *Appl. Phys. Exp.*, vol. 10, no. 1, Jan. 2017, Art. no. 014101, doi: 10.7567/APEX.10.014101.

[119] W. Guo, L. Wang, X. Chen, C. Liu, W. Tang, C. Guo, J. Wang, and W. Lu, "Graphene-based broadband terahertz detector integrated with a square-spiral antenna," *Opt. Lett.*, vol. 43, no. 8, p. 1647, Apr. 2018, doi: 10.1364/OL.43.001647.

[120] K. Zhang, Z. Hu, L. Zhang, Y. Chen, D. Wang, M. Jiang, G. D'Olimpio, L. Han, C. Yao, Z. Chen, H. Xing, C. Kuo, C. S. Lue, I. Vobornik, S. Wang, A. Politano, W. Hu, L. Wang, X. Chen, and W. Lu, "Ultrasensitive self-driven terahertz photodetectors based on low-energy type-II dirac fermions and related van der Waals heterojunctions," *Small*, vol. 19, no. 1, Jan. 2023, Art. no. 2205329, doi: 10.1002/smll.202205329.

[121] Y. Li, Y. Zhang, T. Li, M. Li, Z. Chen, Q. Li, H. Zhao, Q. Sheng, W. Shi, and J. Yao, "Ultrabroadband, ultraviolet to terahertz, and high sensitivity $CH_3NH_3PbI_3$ perovskite photodetectors," *Nano Lett.*, vol. 20, no. 8, pp. 5646–5654, Aug. 2020, doi: 10.1021/acs.nanolett.0c00082.

[122] J. Wang, W. Li, J. Gou, Z. Wu, and Y. Jiang, "Fabrication and parameters calculation of room temperature terahertz detector with microbridge structure," *J. Infr., Millim., THz Waves*, vol. 36, no. 1, pp. 49–59, Jan. 2015, doi: 10.1007/s10762-014-0120-x.

[123] R. Degl'Innocenti, L. Xiao, D. S. Jessop, S. J. Kindness, Y. Ren, H. Lin, J. A. Zeitler, J. A. Alexander-Webber, H. J. Joyce, P. Braeuninger-Weimer, S. Hofmann, H. E. Beere, and D. A. Ritchie, "Fast room-temperature detection of terahertz quantum cascade lasers with graphene-loaded bow-tie plasmonic antenna arrays," *ACS Photon.*, vol. 3, no. 10, pp. 1747–1753, Oct. 2016, doi: 10.1021/acsphotonics.6b00405.

[124] C. Liu, L. Wang, X. Chen, A. Politano, D. Wei, G. Chen, W. Tang, W. Lu, and A. Tredicucci, "Room-temperature high-gain long-wavelength photodetector via optical–electrical controlling of hot carriers in graphene," *Adv. Opt. Mater.*, vol. 6, no. 24, Dec. 2018, Art. no. 1800836, doi: 10.1002/adom.201800836.

[125] M. Chen, Y. Wang, and Z. Zhao, "Localized electromagnetic resonance enabled THz photothermoelectric detection in graphene," *Frontiers Phys.*, vol. 8, p. 216, Jun. 2020, doi: 10.3389/fphy.2020.00216.

[126] O. Mitrofanov, L. Viti, E. Dardanis, M. C. Giordano, D. Ercolani, A. Politano, L. Sorba, and M. S. Vitiello, "Near-field terahertz probes with room-temperature nanodetectors for subwavelength resolution imaging," *Sci. Rep.*, vol. 7, no. 1, p. 44240, Mar. 2017, doi: 10.1038/srep44240.

[127] Z. Shen, X. Ji, Y. Liao, K. Wang, B. Jin, and F. Yan, "Resonant polysilicon antenna for terahertz detection," *IEEE Photon. J.*, vol. 11, no. 4, pp. 1–8, Aug. 2019, doi: 10.1109/JPHOT.2019.2923195.

[128] L. Vicarelli, A. Tredicucci, and A. Pitanti, "Micromechanical bolometers for subterahertz detection at room temperature," *ACS Photon.*, vol. 9, no. 2, pp. 360–367, Feb. 2022, doi: 10.1021/acsphotonics.1c01273.

[129] F. Bianco, D. Perenzoni, D. Convertino, S. L. De Bonis, D. Spirito, M. Perenzoni, C. Coletti, M. S. Vitiello, and A. Tredicucci, "Terahertz detection by epitaxial-graphene field-effect-transistors on silicon carbide," *Appl. Phys. Lett.*, vol. 107, no. 13, Sep. 2015, Art. no. 131104, doi: 10.1063/1.4932091.

[130] L. Viti, A. Politano, K. Zhang, and M. S. Vitiello, "Thermoelectric terahertz photodetectors based on selenium-doped black phosphorus flakes," *Nanoscale*, vol. 11, no. 4, pp. 1995–2002, Jan. 2019, doi: 10.1039/C8NR09060B.

[131] S. Castilla, B. Terrés, M. Autore, L. Viti, J. Li, A. Y. Nikitin, I. Vangelidis, K. Watanabe, T. Taniguchi, E. Lidorikis, M. S. Vitiello, R. Hillenbrand, K.-J. Tielrooij, and F. H. L. Koppens, "Fast and sensitive terahertz detection using an antenna-integrated graphene pn junction," *Nano Lett.*, vol. 19, no. 5, pp. 2765–2773, May 2019, doi: 10.1021/acs.nanolett.8b04171.

[132] L. Viti, D. G. Purdie, A. Lombardo, A. C. Ferrari, and M. S. Vitiello, "HBN-encapsulated, graphene-based, room-temperature terahertz receivers, with high speed and low noise," *Nano Lett.*, vol. 20, no. 5, pp. 3169–3177, May 2020, doi: 10.1021/acs.nanolett.9b05207.

[133] W. Guo, Z. Dong, Y. Xu, C. Liu, D. Wei, L. Zhang, X. Shi, C. Guo, H. Xu, G. Chen, L. Wang, K. Zhang, X. Chen, and W. Lu, "Sensitive terahertz detection and imaging driven by the photothermoelectric effect in ultrashort-channel black phosphorus devices," *Adv. Sci.*, vol. 7, no. 5, Mar. 2020, Art. no. 1902699, doi: 10.1002/advs.201902699.

[134] J. A. Arnaud, W. M. Hubbard, G. D. Mandeville, B. de la Clavière, E. A. Franke, and J. M. Franke, "Technique for fast measurement of Gaussian laser beam parameters," *Appl. Opt.*, vol. 10, no. 12, p. 2775, Dec. 1971, doi: 10.1364/AO.10.002775.

[135] D. A. Fish, J. G. Walker, A. M. Brinicombe, and E. R. Pike, "Blind deconvolution by means of the Richardson–Lucy algorithm," *J. Opt. Soc. Amer. A, Opt. Image Sci.*, vol. 12, no. 1, p. 58, Jan. 1995, doi: 10.1364/JOSAA.12.000058.

[136] Q. Mao, X. Tu, L. Xu, C. Wan, L. Kang, J. Chen, and P. Wu, "Effective receiving area of the antenna-coupled terahertz detector," *Opt. Eng.*, vol. 53, no. 2, Feb. 2014, Art. no. 023103, doi: 10.1117/1.OE.53.2.023103.

[137] I. Ryger, P. Lobotka, A. Steiger, S. Chromik, T. Lalinsky, Z. Raida, K. Pítra, J. Zehetner, M. Spankova, S. Gazi, M. Sojkova, and G. Vanko, "Uncooled antenna-coupled microbolometer for detection of terahertz radiation," *J. Infr., Millim., THz Waves*, vol. 42, no. 4, pp. 462–478, Apr. 2021, doi: 10.1007/s10762-021-00781-y.

[138] S. A. Kuznetsov, A. G. Paulish, M. Navarro-Cía, and A. V. Arzhannikov, "Selective pyroelectric detection of millimetre waves using ultra-thin metasurface absorbers," *Sci. Rep.*, vol. 6, no. 1, p. 21079, Feb. 2016, doi: 10.1038/srep21079.

[139] S.-P. Han, H. Ko, J.-W. Park, N. Kim, Y.-J. Yoon, J.-H. Shin, D. Y. Kim, D. H. Lee, and K. H. Park, "InGaAs Schottky barrier diode array detector for a real-time compact terahertz line scanner," *Opt. Exp.*, vol. 21, no. 22, p. 25874, Nov. 2013, doi: 10.1364/OE.21.025874.

[140] S. M. Rahman, Z. Jiang, M. I. B. Shams, P. Fay, and L. Liu, "A G-band monolithically integrated quasi-optical zero-bias detector based on heterostructure backward diodes using submicrometer airbridges," *IEEE Trans. Microw. Theory Techn.*, vol. 66, no. 4, pp. 2010–2017, Apr. 2018, doi: 10.1109/TMTT.2017.2779133.

[141] H. Qin, X. Li, J. Sun, Z. Zhang, Y. Sun, Y. Yu, X. Li, and M. Luo, "Detection of incoherent terahertz light using antenna-coupled high-electron-mobility field-effect transistors," *Appl. Phys. Lett.*, vol. 110, no. 17, Apr. 2017, Art. no. 171109, doi: 10.1063/1.4982604.

[142] Y. Zhang, S. Hosono, N. Nagai, S.-H. Song, and K. Hirakawa, "Fast and sensitive bolometric terahertz detection at room temperature through thermomechanical transduction," *J. Appl. Phys.*, vol. 125, no. 15, Apr. 2019, Art. no. 151602, doi: 10.1063/1.5045256.

[143] J. Sun, Y. Zhu, W. Feng, Q. Ding, H. Qin, Y. Sun, Z. Zhang, X. Li, J. Zhang, X. Li, Y. Shangguan, and L. Jin, "Passive terahertz imaging detectors based on antenna-coupled high-electron-mobility transistors," *Opt. Exp.*, vol. 28, no. 4, p. 4911, Feb. 2020, doi: 10.1364/OE.385042.

[144] K. Ikamas, D. B. But, and A. Lisauskas, "Homodyne spectroscopy with broadband terahertz power detector based on 90-nm silicon CMOS transistor," *Appl. Sci.*, vol. 11, no. 1, p. 412, Jan. 2021, doi: 10.3390/app11010412.

[145] R. Müller, B. Gutschwager, J. Hollandt, M. Kehrt, C. Monte, R. Müller, and A. Steiger, "Characterization of a large-area pyroelectric detector from 300 GHz to 30 THz," *J. Infr., Millim., THz Waves*, vol. 36, no. 7, pp. 654–661, Jul. 2015, doi: 10.1007/s10762-015-0163-7.

[146] A. Zak, M. A. Andersson, M. Bauer, J. Matukas, A. Lisauskas, H. G. Roskos, and J. Stake, "Antenna-integrated 0.6 THz FET direct detectors based on CVD graphene," *Nano Lett.*, vol. 14, no. 10, pp. 5834–5838, 2014, doi: 10.1021/nl5027309.

[147] M. Ferreras, D. Cibiraite-Lukenskiene, A. Lisauskas, J. Grajal, and V. Krozer, "Broadband sensing around 1 THz via a novel biquad-antenna-coupled low-NEP detector in CMOS," *IEEE Trans. THz Sci. Technol.*, vol. 11, no. 1, pp. 16–27, Jan. 2021, doi: 10.1109/TTHZ.2020.3031483.

[148] Y. Takida, S. Suzuki, M. Asada, and H. Minamide, "Sensitive terahertz-wave detector responses originated by negative differential conductance of resonant-tunneling-diode oscillator," *Appl. Phys. Lett.*, vol. 117, no. 2, Jul. 2020, Art. no. 021107, doi: 10.1063/5.0012318.

[149] A. A. Generalov, M. A. Andersson, X. Yang, A. Vorobiev, and J. Stake, "A 400-GHz graphene FET detector," *IEEE Trans. THz Sci. Technol.*, vol. 7, no. 5, pp. 614–616, Sep. 2017, doi: 10.1109/TTHZ.2017.2722360.

[150] X. Yang, A. Vorobiev, A. Generalov, M. A. Andersson, and J. Stake, "A flexible graphene terahertz detector," *Appl. Phys. Lett.*, vol. 111, no. 2, Jul. 2017, Art. no. 021102, doi: 10.1063/1.4993434.

[151] P. Xiao, X. Tu, L. Kang, C. Jiang, S. Zhai, Z. Jiang, D. Pan, J. Chen, X. Jia, and P. Wu, "Reflective grating-coupled structure improves the detection efficiency of THz array detectors," *Sci. Rep.*, vol. 8, no. 1, pp. 1–12, May 2018, doi: 10.1038/s41598-018-26204-y.

[152] J. Tong, M. Muthee, S.-Y. Chen, S. K. Yngvesson, and J. Yan, "Antenna enhanced graphene THz emitter and detector," *Nano Lett.*, vol. 15, no. 8, pp. 5295–5301, Aug. 2015, doi: 10.1021/acs.nanolett.5b01635.

[153] S. Boppel, M. Ragauskas, A. Hajo, M. Bauer, A. Lisauskas, S. Chevtchenko, A. Ramer, I. Kasalynas, G. Valusis, H.-J. Wurfl, W. Heinrich, G. Trankle, V. Krozer, and H. G. Roskos, "0.25-GaN TeraFETs optimized as THz power detectors and intensity-gradient sensors," *IEEE Trans. THz Sci. Technol.*, vol. 6, no. 2, pp. 348–350, Mar. 2016, doi: 10.1109/TTHZ.2016.2520202.

[154] X. Yang, A. Vorobiev, J. Yang, K. Jeppson, and J. Stake, "A linear-array of 300-GHz antenna integrated GFET detectors on a flexible substrate," *IEEE Trans. THz Sci. Technol.*, vol. 10, no. 5, pp. 554–557, Sep. 2020, doi: 10.1109/TTHZ.2020.2997599.

[155] C. Daher, J. Torres, I. Iniguez-de-la-Torre, P. Nouvel, L. Varani, P. Sangare, G. Ducournau, C. Gaquiere, J. Mateos, and T. Gonzalez, "Room temperature direct and heterodyne detection of 0.28–0.69-THz waves based on GaN 2-DEG unipolar nanochannels," *IEEE Trans. Electron Devices*, vol. 63, no. 1, pp. 353–359, Jan. 2016, doi: 10.1109/TED.2015.2503987.

[156] D. A. Bandurin, I. Gayduchenko, Y. Cao, M. Moskotin, A. Principi, I. V. Grigorieva, G. Goltsman, G. Fedorov, and D. Svintsov, "Dual origin of room temperature sub-terahertz photoresponse in graphene field effect transistors," *Appl. Phys. Lett.*, vol. 112, no. 14, Apr. 2018, Art. no. 141101, doi: 10.1063/1.5018151.

[157] X. Yang, A. Vorobiev, K. Jeppson, and J. Stake, "Describing broadband terahertz response of graphene FET detectors by a classical model," *IEEE Trans. THz Sci. Technol.*, vol. 10, no. 2, pp. 158–166, Mar. 2020, doi: 10.1109/TTHZ.2019.2960678.

[158] I. Gayduchenko, S. G. Xu, G. Alymov, M. Moskotin, I. Tretyakov, T. Taniguchi, K. Watanabe, G. Goltsman, A. K. Geim, G. Fedorov, D. Svintsov, and D. A. Bandurin, "Tunnel field-effect transistors for sensitive terahertz detection," *Nature Commun.*, vol. 12, no. 1, p. 543, Jan. 2021, doi: 10.1038/s41467-020-20721-z.

[159] S. Bevilacqua and S. Cherednichenko, "Low noise nanometer scale room-temperature $YBa_2Cu_3O_{7-x}$ bolometers for THz direct detection," *IEEE Trans. THz Sci. Technol.*, vol. 4, no. 6, pp. 653–660, Nov. 2014, doi: 10.1109/TTHZ.2014.2344435.

[160] H. Ito and T. Ishibashi, "Low-noise terahertz-wave detection by InP/InGaAs Fermi-level managed barrier diode," *Appl. Phys. Exp.*, vol. 9, no. 9, Sep. 2016, Art. no. 092401, doi: 10.7567/APEX.9.092401.

[161] D. Cibiraite-Lukenskiene, K. Ikamas, and T. Lisauskas, "Passive detection and imaging of human body radiation using an uncooled field-effect transistor-based THz detector," *Sensors*, vol. 20, p. 4087, Jan. 2020, doi: 10.3390/s20154087.

[162] A. Rogalski, "Progress in performance development of room temperature direct terahertz detectors," *J. Infr., Millim., THz Waves*, vol. 43, nos. 9–10, pp. 709–727, Sep. 2022, doi: 10.1007/s10762-022-00882-2.

[163] D. B. Rutledge and M. S. Muha, "Imaging antenna arrays," *IEEE Trans. Antennas Propag.*, vol. AP-30, no. 4, pp. 535–540, Jul. 1982, doi: 10.1109/TAP.1982.1142856.

[164] K. Zhou, W. Miao, B. Fan, Y. Delorme, S. Caroopen, M. Batrung, and S. Shi, "Transmittance of high-density polyethylene from 0.1 THz to 15 THz," *Proc. SPIE*, vol. 11196, p. 33, Nov. 2019, doi: 10.1117/12.2534490.

[165] J. Grzyb, M. Andree, R. Jain, B. Heinemann, and U. R. Pfeiffer, "A lens-coupled on-chip antenna for dual-polarization SiGe HBT THz direct detector," *IEEE Antennas Wireless Propag. Lett.*, vol. 18, no. 11, pp. 2404–2408, Nov. 2019, doi: 10.1109/LAWP.2019.2927300.

[166] A. Boukhayma, A. Dupret, J.-P. Rostaing, and C. Enz, "A low-noise CMOS THz imager based on source modulation and an in-pixel high-Q passive switched-capacitor N-path filter," *Sensors*, vol. 16, no. 3, p. 325, Mar. 2016, doi: 10.3390/s16030325.

[167] *VDI PM5B Operational Manual*. Accessed: Jan. 12, 2023. [Online]. Available: https://www.vadiodes.com/images/Products/PowerMeter/PM5manual/VDI-724.1_PM5B_Manual.pdf

[168] T. Keating. *THz Absolute Power & Energy Meter System*. [Online]. Available: http://www.terahertz.co.uk/images/tki/PMETER/TKPOWERMETERMANUAL3p2p2.pdf (Accessed: Jan. 12, 2023).

[169] Scientech. *Vector Series Models H410 & H410D*. Accessed: Jan. 12, 2023. [Online]. Available: https://scientech-Inc.com/media/downloadable/files/links/1/0/10795t_vector_h410_op_manual.pdf

[170] Keysight. *Power Meters and Power Sensors*. Accessed: Jan. 12, 2023. [Online]. Available: https://www.keysight.com/us/en/assets/7018-01513/brochures/5989-6240.pdf

[171] Tydex. *Golay Detectors*. Accessed: Jan. 12, 2023. [Online]. Available: https://www.tydexoptics.com/pdf/Golay_Detectors.pdf

[172] Gentec EO. *Spectrum / Gentec-Eo*. Accessed: Jan. 12, 2023. [Online]. Available: https://www.gentec-eo.com/content/uploads/spectrum/cross-reference_product_list_2016_v1.0.pdf

[173] Ophir. *High Sensitivity Thermal Sensors*. Accessed: Jan. 12, 2023. [Online]. Available: https://www.ophiropt.com/laser–measurement/sites/default/files/3A-P-THz_3A-FS_3A-P-FS-12.pdf

ARIE PANGESTI AJI was born in Bandung, Indonesia, in 1987. He received the B.A.Sc. degree in telecommunication engineering from Politeknik Elektronika Negeri Surabaya, in 2009, the M.E. degree in electrical engineering from Universitas Indonesia, in 2018, and the Ph.D. degree in nano vision technology from Shizuoka University, in 2022. His research interests include terahertz engineering, antenna design and optimization, and microwave technology.

CATUR APRIONO (Member, IEEE) received the B.Eng. and M.Eng. degrees in telecommunication engineering from the Department of Electrical Engineering, Universitas Indonesia, Indonesia, in 2009 and 2011, respectively, and the Ph.D. degree in nano vision technology from Shizuoka University, Japan, in 2015.

Since 2018, he has been an Assistant Professor of telecommunication engineering with Universitas Indonesia, where he is currently a Lecturer with the Department of Electrical Engineering, Faculty of Engineering. His main research interests include antenna and microwave engineering, terahertz wave technology, and optical communications. He was a member of the IEEE Antenna and Propagation Society (AP-S) and the IEEE Microwave Theory and Technique Society (MTT-S). He was a Secretary and a Treasurer of the IEEE Joint Chapter MTT/AP Indonesia Section, in 2017, 2018, and 2019. He is active in various chapter activities, such as the First Indonesia–Japan Workshop on Antennas and Wireless Technology (IJAWT) as a Secretary and the 2019 IEEE International Conference on Antenna Measurements Applications (CAMA), Bali, in October 2019, as a Treasurer.

EKO TJIPTO RAHARDJO (Member, IEEE) was born in Pati, Indonesia, in 1958. He received the Ir. degree in electrical engineering from Universitas Indonesia, Depok, Indonesia, in 1981, the M.S. degree in electrical engineering from the University of Hawai'i at Manoa, Honolulu, HI, USA, in 1987, and the Ph.D. degree in electrical engineering from Saitama University, Urawa, Japan, in 1996.

Since 1982, he has been a Teaching Assistant with the Department of Electrical Engineering, Universitas Indonesia. Since 2005, he has been a Professor of electrical engineering. He was the Chairperson of University Senate, Universitas Indonesia, from 2011 to 2012; the Head of the Department of Electrical Engineering, Universitas Indonesia, from 2004 to 2008; and the Executive Director of the Quality Undergraduate Education (QUE), Department of Electrical Engineering, Universitas Indonesia, from 1999 to 2004, where he was also the Head of the Telecommunication Laboratory, from 1997 to 2004. Since 2003, he has been the Director of the Antenna Propagation and Microwave Research Group (AMRG), Universitas Indonesia. He has published and presented more than 100 research articles in national and international journals and symposiums. His research interests include antenna engineering, wave propagation, microwave circuits, communication systems, and telecommunications system regulation.

Prof. Rahardjo is a member of the IEEE Antenna and Propagation Society (AP-S) and IEEE Microwave Theory and Technique Society (MTTS). He has been a member of the International Steering Committee (ISC) of the Asia–Pacific Microwave Conference (APMC), since 2010, and the International Advisory Board of the International Symposium on Antenna and Propagation (ISAP), since 2012. He received the Indonesian Government Scholarship through MUCIA, from 1984 to 1987, the Hitachi Scholarship, from 1992 to 1996, the Young Researcher's Award from Universitas Indonesia, in 1996, the second winner of the Best Researcher Award in Science and Technology from Universitas Indonesia, in 2009, and the second winner of the Best Teaching Award from Universitas Indonesia, in 2010. He was the Founder of the IEEE Joint Chapter MTTS/AP-S, Indonesia. He has served as the President for the IEEE Joint Chapter MTT-S/AP-S, from 2009 to 2010, and the IEEE Indonesia Section, from 2014 to 2015. He was the General Chairperson of the Indonesia–Malaysia Microwave and Antenna Conference (IMMAC), Depok, in 2010 and the Indonesia–Japan Joint Scientific Symposium (IJJSS), Bali, in 2010; and the General Co-Chairperson of the Indonesia–Japan Joint Scientific Symposium (IJJSS), Chiba, Japan, in 2012. In addition, he was the General Chair of the first Indonesia–Japan Workshop on Antennas and Wireless Technology (IJAWT), Depok, in 2017, and the 2019 IEEE International Conference on Antenna Measurements and Applications (CAMA), Bali, in October 2019.